Origin and evolution of a cold-based tropical mountain glacier on Mars: The Pavonis Mons fan-shaped deposit

David E. Shean and James W. Head
Department of Geological Sciences, Brown University, Providence, Rhode Island, USA

David R. Marchant
Department of Earth Sciences, Boston University, Boston, Massachusetts, USA

Received 13 September 2004; revised 5 January 2005; accepted 22 February 2005; published 5 May 2005.

[1] Each of the large Tharsis Montes volcanoes in the equatorial region of Mars has an unusual Amazonian-aged fan-shaped deposit on its west-northwestern flank. On the basis of Viking Orbiter data, the origin of these deposits has been variously ascribed to volcanic, mass-wasting, tectonic, and glacial processes. Using new MGS and Odyssey data, combined with recent developments in the study of cold-based glaciers, we reassess the geology and mode of origin for these deposits with particular emphasis on Pavonis Mons. The deposits share three characteristic facies, including (1) a ridged facies, consisting of tens to >100 parallel, concentric ridges around the margins of the deposits, (2) a knobby facies composed of irregular hills and hummocks, and (3) a smooth facies of broad, lobate plains that superposes all other units within the deposits. On the basis of morphology, topography, superposition relationships, and close terrestrial analogs in the Dry Valleys of Antarctica, we interpret the Pavonis fan-shaped deposit as the depositional remains of a cold-based glacier that formed on the northwestern flank in recent Martian history. We interpret the ridged facies as drop moraines formed around the margins of a retreating cold-based glacier, the knobby facies as a sublimation till derived from in situ down-wasting of cold-based glacial ice, and the smooth facies as extant debris-covered glacial ice. In addition to the three main facies, the fan-shaped deposit at Pavonis Mons contains several unique features, including arcuate scarps, high-relief flow-like features, and radial ridges, which suggest that volcanism played a role during its formation. Using recent results from Mars general circulation model simulations, we outline a model of glacier formation involving atmospheric deposition of water ice on the northwestern flanks of the Tharsis Montes during periods of high mean obliquity. Reconstructed ice sheet profiles for each of the Tharsis Montes glaciers suggest that the ice sheets attained average thicknesses of ~1.6–2.4 km, values that are consistent with a cold-based glacial origin. Analysis of crater size-frequency distributions using new data indicates that the age of the glaciation lies within the Late Amazonian (~10–200 Ma). Thus our results suggest that multiple phases of tropical mountain glaciation occurred on Mars within the past few hundred Myr and that significant amounts of near-surface, equatorial ice may remain within the deposit today.

Citation: Shean, D. E., J. W. Head, and D. R. Marchant (2005), Origin and evolution of a cold-based tropical mountain glacier on Mars: The Pavonis Mons fan-shaped deposit, *J. Geophys. Res.*, *110*, E05001, doi:10.1029/2004JE002360.

1. Introduction

1.1. Location and Setting of Fan-Shaped Deposits

[2] The Tharsis Rise is a large equatorial province on Mars characterized by large-scale volcanic and tectonic features. Three 14.0–18.0 km high, relatively young shield volcanoes cap the Tharsis Rise, collectively known as the Tharsis Montes (Arsia Mons, Pavonis Mons and Ascraeus Mons). On the basis of crater counts, the Tharsis Montes are considered to have formed during the Late-Hesperian through the Late Amazonian period of Mars history [*Scott and Tanaka*, 1986]. Each of the Tharsis Montes volcanoes has a fan-shaped deposit located to the west-northwest of the shield (Figure 1). These fan-shaped deposits generally share three main facies, including a ridged facies, a knobby facies, and a smooth facies [*Zimbelman and Edgett*, 1992]. The deposit at Arsia Mons is considered to be the foremost example of the three because of its well-defined characteristic units and their clear-cut relationships within the deposit (Figure 2) [*Scott and Zimbelman*, 1995; *Head and Marchant*, 2003]. The Pavonis Mons fan-shaped

0148-0227/05/2004JE002360$09.00

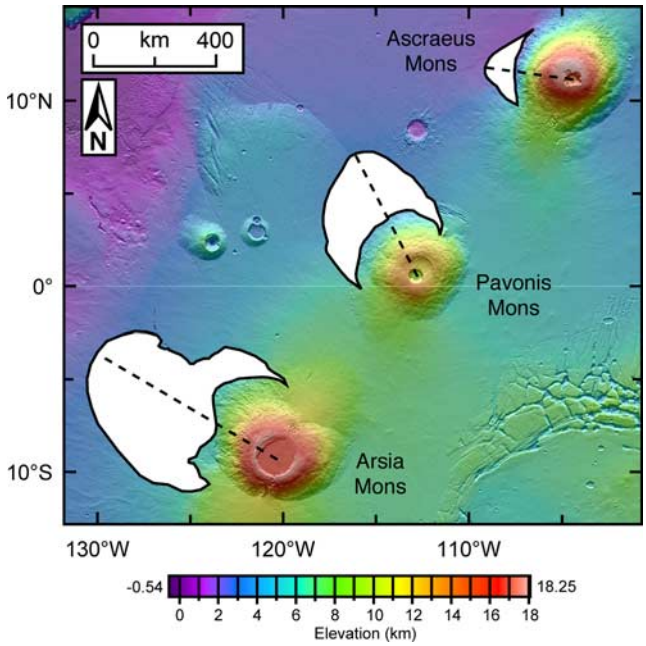

Figure 1. MOLA topography data (128 pixels/degree) of Tharsis Montes over shaded relief map with a simple cylindrical projection. The Tharsis Montes fan-shaped deposits (mapped as white regions with solid outline) are present to the west-northwest of each shield. The dashed line connecting the caldera center and most distal edge of each deposit represents the location of the MOLA profiles extracted for the ice sheet models in section 4 and Figure 28. Note the broad topographic rise present to the west of the Pavonis fan-shaped deposit.

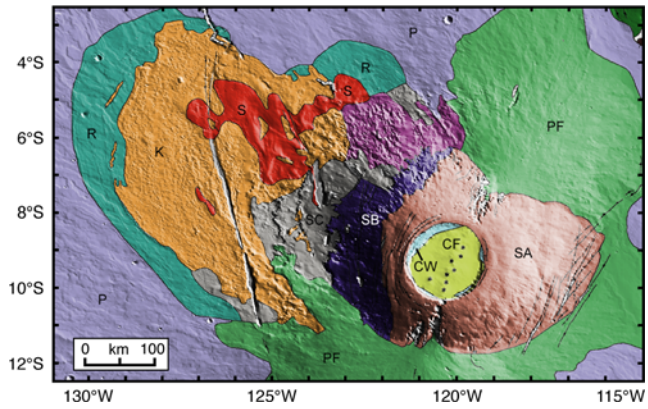

Figure 2. Geologic map of Arsia Mons and associated fan-shaped deposit modified from *Zimbelman and Edgett* [1992] by *Head and Marchant* [2003] superposed on MOLA shaded relief map. The three characteristic units of the Tharsis Montes fan-shaped deposits are present within the Arsia deposit, including the ridged facies (R) around the margins of the deposit, the knobby facies (K) in the proximal regions, and the smooth facies (S) superposed on all other units. Other units include shield (SA), degraded western flank (SB), smooth lower western flank (SC), caldera floor (CF), caldera wall (CW), flank vent flows (PF), and undivided Tharsis Plains (P).

deposit shares many similarities with the Arsia deposit [*Zimbelman and Edgett*, 1992; *Scott et al.*, 1998], with several unique features that justify further analysis and a reevaluation of previous interpretations for the fan-shaped deposits and their history. Finally, the Ascraeus Mons fan-shaped deposit is notably less extensive than the deposit at Arsia or Pavonis; however, it does contain similar geologic features [*Zimbelman and Edgett*, 1992; *Parsons and Head*, 2004]. A smaller, multilobate fan-shaped deposit is also present to the west and northwest of the Olympus Mons basal scarp [*Lucchitta*, 1981; *Milkovich and Head*, 2003; *Neukum et al.*, 2004; *Head et al.*, 2005]. Table 1 summarizes the pertinent quantitative data for the Tharsis Montes fan-shaped deposits.

1.2. Previous Analyses of the Fan-Shaped Deposits

[3] Any explanation for the origin of the fan-shaped deposits must take into account both the similarities and differences in their morphologies, their approximately similar Amazonian age, and the fact that all three are present on the west-northwestern sides of the volcanoes [*Edgett*, 1989]. On the basis of Viking Orbiter data, several explanations for their origin have been proposed, including (1) gravity-driven mass wasting (landslides, volcanic-debris avalanches, lahars), (2) erosional features and debris from glaciation, (3) volcanism (pyroclastic flows, ash flows), and (4) deformation of the terrain northwest of the Tharsis Montes.

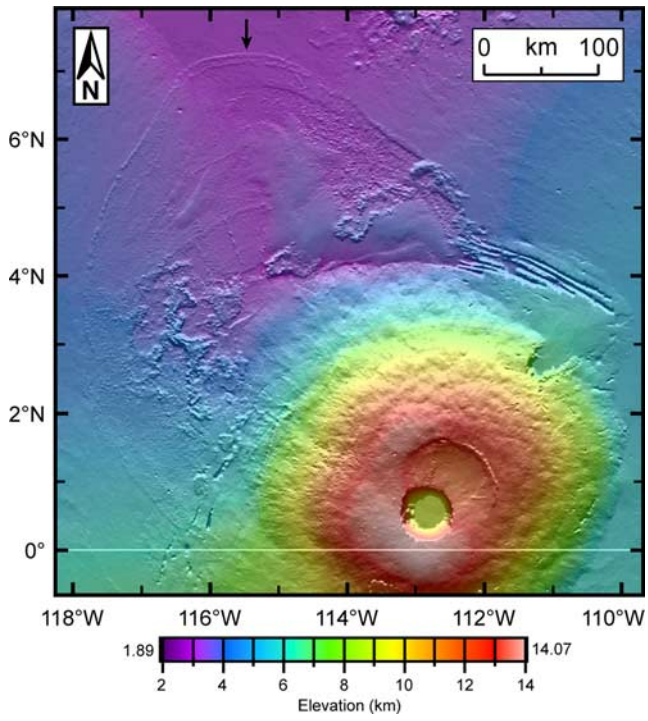

Figure 3. MOLA shaded relief map of Pavonis Mons and fan-shaped deposit with color overlay. Note the large outer ridges that define the margins of the deposit (arrow highlights the large outer ridge that defines the northern margin of the deposit), the expansive smooth facies, and unique lobate flow-like features in the western regions of the deposit.

Table 1. Quantitative Data for the Tharsis Montes Fan-Shaped Deposits

	Arsia	Pavonis	Ascraeus
Surface area, km^2	180,000	75,000	14,000
Trend	N62°W	N27°W	N82°W
Lowest elevation of deposit, km	2.7	2.8	1.5
Highest elevation of deposit, km	7.0	8.5	5.5
Maximum elongation, km	450	235	100

[4] Several models suggest that the fan-shaped deposits are the result of massive landslides originating on the flanks of the shield [e.g., *Carr et al.*, 1977; *Scott and Tanaka*, 1981, 1986; *Edgett and Zimbelman*, 1987; *Morris et al.*, 2003]. However, there are several problems with this scenario, and many features within the deposit cannot be explained by the landslide hypothesis. For example, the average slope of the lower flanks at Pavonis Mons where the landslide would have originated is approximately 3°, while subaerial terrestrial landslides have not been documented for slopes less than 13° [*Edgett*, 1989]. In addition, the reduced gravity field on Mars would require significantly higher slopes or a substantial lubricant to sustain landslides of this magnitude. Estimates for runout length (L) as a function of vertical drop (H) show H/L ratios ranging from 0.01–0.02 [*Scott and Zimbelman*, 1995]. Typical terrestrial landslides or debris avalanches have considerably higher ratios of 0.2 and 0.1, respectively [*Scott and Zimbelman*, 1995]. The uniform nature of the ridged and knobby facies is also inconsistent with a landslide hypothesis. At Arsia Mons, the ridges do not become progressively more fragmented, nor do they decrease in size, spacing or number with greater distance from the volcano as would be expected with a landslide or debris-flow [*Scott and Zimbelman*, 1995]. Furthermore, the Pavonis fan-shaped deposit is observed at elevations of nearly 8.5 km on the northeastern flanks and 6.5 km on the southwestern flanks of the shield. There is no scarp or headwall at these elevations and no evidence for mass-wasting events that could account for the volume of material necessary to produce the fan-shaped deposit during a catastrophic slide.

[5] As an alternative to the mass-wasting models, *Williams* [1978] and *Lucchitta* [1981] developed a glacial hypothesis, suggesting that the fan-shaped deposits were "moraines [deposited] due to recession of local ice caps that formed on the volcanoes from mixtures of emanated volatiles and erupted ash" [*Lucchitta*, 1981]. This model is based on parallels drawn between the fan-shaped deposit at Arsia Mons and terrestrial glacial features, such as those observed in Iceland [*Lucchitta*, 1981]. On the basis of morphological relations, this model suggests that the ridged facies at Arsia Mons may be a series of washboard moraines deposited at the margins of a retreating glacier [*Williams*, 1978; *Lucchitta*, 1981]. *Lucchitta* [1981] also notes that other features within fan-shaped deposits are closely associated with glacier or rock glacier morphologies. It is important to note that as part of the *Lucchitta* [1981] model, volcanic eruptions from each of the Tharsis Montes are cited as the source for the water necessary to produce these glaciers. *Grizzaffi and Schultz* [1989] compare the ridged facies of the Arsia Mons fan-shaped deposit to a series of curvilinear ridges and hillocky terrain within the Isidis basin. They suggest that the ridges at Arsia and Isidis may be the result of volatile precipitation and aerial deposition of debris followed by eolian erosion and sublimation to leave the ridges [*Grizzaffi and Schultz*, 1989]. *Helgason* [1999] also supported a glacial origin for the fan-shaped deposits and suggested that the knobby facies at Arsia Mons represents dead-ice with a relatively thin cover of wind-blown dust.

[6] One of the main arguments against a glacial origin involves the difficulties associated with forming such large water ice concentrations at equatorial latitudes on Mars. Under current climate conditions, surface water ice is not stable at these latitudes [*Farmer and Doms*, 1979]. *Scott and Zimbelman* [1995] also note that such thick glaciers would be expected to produce evidence of downslope basal scouring which is not observed on the flanks of the Tharsis Montes.

[7] Others have suggested that a combination of glacial and volcanic processes can account for the emplacement of the fan-shaped deposits at both Arsia and Pavonis Mons [e.g., *Scott and Zimbelman*, 1995; *Scott et al.*, 1998]. Using Viking Orbiter data of Pavonis Mons, *Scott et al.* [1998] mapped the ridged facies as recessional moraines, the knobby facies as landforms developed beneath the wastage zone of a disintegrating ice sheet and the smooth facies as ash flow tuffs or lahars. The smooth facies at Pavonis Mons has also been interpreted as a pyroclastic deposit, which emanated from large troughs off the northern flank [*Zimbelman and Edgett*, 1992].

[8] On the basis of their initial observations of Viking Orbiter data, *Carr et al.* [1977] proposed an alternative to their landslide hypothesis, suggesting that the fan-shaped deposit at Arsia might be a large ash flow deposit. The results of radar surveys (3.5 cm wavelength) during the 1988 Mars opposition revealed a "stealth region" which occupies the western slopes of Pavonis Mons and Arsia Mons [*Muhleman et al.*, 1991]. In an attempt to explain the radar anomaly, *Edgett et al.* [1996] suggested that features within the fan-shaped deposits were the result of postcaldera pyroclastic eruptions on the western flanks of the shields. However, there are several difficulties associated with an entirely volcanic origin, including the lack of large-scale pyroclastic features on the volcano flanks and the failure to explain the location of the deposits exclusively to the northwest or the morphology of the ridged facies [*Carr et al.*, 1977]. Furthermore, the "stealth region" extends over 1000 km to the west of the Tharsis Montes, well beyond the fan-shaped deposits, and it does not include the deposit of Ascraeus Mons, arguing against a direct relationship with the deposits.

[9] Finally, it has been suggested that the ridged facies of the fan-shaped deposits may be the result of deformational events involving low-angle thrust faulting [*Carr et al.*, 1977] or a series of closely spaced folds [*Carr et al.*, 1977; *Anguita and Moreno*, 1992]. However, these models fail to explain the relationships between the three distinct facies within the fan-shaped deposits and the fact that the ridged facies appears to be passively deposited over underlying topographic features.

[10] We have reexamined the Tharsis Montes fan-shaped deposits using new Mars Global Surveyor and Mars Odyssey data in conjunction with the previous Viking Orbiter data. As a result of this investigation, we propose a new glacial

model to explain the fan-shaped deposit at Pavonis Mons. We have expanded on previous studies [e.g., *Williams*, 1978; *Lucchitta*, 1981; *Grizzaffi and Schultz*, 1989; *Scott and Zimbelman*, 1995; *Scott et al.*, 1998], which identified many interesting features within the fan-shaped deposits, but were based entirely on Viking Orbiter data. Our analysis, together with an assessment of cold-based glacial terrestrial analogs [*Head and Marchant*, 2003] lead us to conclude that the fan-shaped deposit at Pavonis Mons is the result of a cold-based glacier that formed on the northwestern flank and advanced onto the surrounding plains in recent Martian history. By building on previous, glacial models [e.g., *Williams*, 1978; *Lucchitta*, 1981; *Grizzaffi and Schultz*, 1989; *Scott and Zimbelman*, 1995; *Scott et al.*, 1998] and incorporating new data, we offer new interpretations of features within the Pavonis Mons fan-shaped deposit, suggesting that multiple phases of glaciation have occurred, direct lava-ice interaction has taken place, and significant volumes of ice may still remain within the deposit today.

2. Data Sets and Methods

[11] A geographical information system (GIS) database was compiled using ESRI's ArcGIS Desktop 8.3, including the following data sets for the Tharsis Montes fan-shaped deposits: (1) 128 pixel/degree gridded Mars Orbiter Laser Altimeter (MOLA) topography data (463 meters/pixel); (2) MOLA point data (~300 m spacing between points along each orbit); (3) 256 pixel/degree Mars Orbiter Camera (MOC) wide-angle camera mosaic (231 meters/pixel); (4) MOC narrow-angle images (1.5–12 meters/pixel); (5) Viking high-resolution image mosaics (50–200 meters/pixel); (6) THEMIS daytime and nighttime infrared data (band 9, 100 meters/pixel); and (7) THEMIS visible image data (band 3, 19 meters/pixel).

[12] From the MOLA topography, several new data sets were generated including shaded-relief maps, slope maps, detrended maps, and aspect maps to further aide in data analysis. Individual MOLA profiles were used in the analysis where more detailed local topography was required. A new geologic map of the units and features within the Pavonis fan-shaped deposit was also generated within ArcMap.

[13] In order to produce mosaics of THEMIS infrared and visible data, a custom procedure was written to execute a series of commands for Integrated Software for Imagers and Spectrometers (ISIS). These scripts automatically process raw THEMIS data from level 0 (uncorrected and unprojected) to level 4 (corrected and map-projected), producing equalized mosaics with image seams removed.

3. Pavonis Mons Fan-Shaped Deposit

[14] The Pavonis fan-shaped deposit (Figures 3–6) extends approximately 250 km northwest of the base of the shield along a N27°W trend (Figure 1) and is emplaced on the Tharsis Plains unit consisting of Amazonian flows from Pavonis and Arsia Mons [*Scott and Tanaka*, 1986]. The deposit at Pavonis Mons has maximum dimensions of ~375 × 420 km and covers an area of >75,000 km^2, equivalent to about 42% of the area covered by the Arsia fan-shaped deposit [*Head and Marchant*, 2003] (Table 1).

[15] The Mars Orbiter Laser Altimeter (MOLA) instrument aboard the Mars Global Surveyor (MGS) spacecraft has provided high-resolution altimetry data for Mars on a global scale [*Smith et al.*, 1999, 2001], and as a result, new information about the Pavonis fan-shaped deposit (Figure 3). For example, we now know that the Pavonis Mons shield reaches elevations of approximately 14.0 km above Mars datum with an average slope of around 5° on the upper flanks and an average slope of approximately 3° on the lower flanks (Figure 7). Two large elongated rift zones are present on the northeast and the southwest flanks of Pavonis Mons (Figures 1 and 3), along the apparent N40°E trending fissure through the Tharsis Montes [*Crumpler and Aubele*, 1978]. The fan-shaped deposit attains elevations of nearly 8.5 km on the northeastern flanks of the shield, where the deposit is draped over *Pavonis Fossae*, a series of large graben that cut through the late-stage northeastern flank vent flows at Pavonis (Figure 8). The lowest observed elevations for the Pavonis fan-shaped deposit are about 2.8 km above Mars datum at the north-northwestern margin of the deposit (Figures 3 and 7).

[16] On the Tharsis Plains to the north of the shield, slopes are gentle (<0.3°) and generally trend to the northwest (Figure 1). A broad topographic rise (Figure 1) is also present to the west of Pavonis Mons. This rise is characterized by a relatively flat central plateau with margins attaining slopes of ~2°. Individual digitate lava flows can be discerned within the rise through analysis of MOLA shaded relief maps (Figure 3), detrended MOLA data and THEMIS daytime IR images. The western half of the Pavonis fan-shaped deposit is emplaced on this rise up to elevations of >5.0 km (Figure 3). Along the northern edge of the rise, a series of shallow graben are observed within the rise and the underlying plains (Figure 4). These graben are concentric to the margins of the topographic rise and some can be traced beneath the fan-shaped deposit for >110 km.

[17] It appears that the topographic rise played a role during the emplacement of the fan-shaped deposit at Pavonis, skewing the overall shape toward the north (Figures 1 and 3) and producing an "indentation" of the deposit over the rise in plan view. It is interesting to note that despite an apparently similar regional slope of <0.5–1.0° to the northwest at all three of the Tharsis Montes [*Zimbelman and Edgett*, 1992], the fan-shaped deposit at Pavonis Mons has a much more northerly trend of N27°W when compared to the more westerly-trending deposits at Arsia (N62°W) and Ascraeus (N82°W) (Figure 1, Table 1). We propose that the anomalous trend of the Pavonis deposit may be directly related to the topographic rise to the west of the shield, which is not a factor at either Arsia or Ascraeus.

[18] MOLA topography data also reveal three arcuate scarps within the Pavonis fan-shaped deposit (Figure 4). One of these scarps, referred to here as the eastern scarp, is concentric to and approximately 5–10 km within the eastern margin of the Pavonis fan-shaped deposit (Figure 4). This scarp has a relief of >250 m in places and extends for >80 km. Another scarp with a relief of up to 100 m and length of >120 km, termed the inner eastern scarp, is observed approximately 20–30 km from and concentric to the northeastern margins of the fan-shaped deposit (Figure 4). Finally, a third arcuate scarp (termed the western scarp) with a relief of up to 350 m and length of

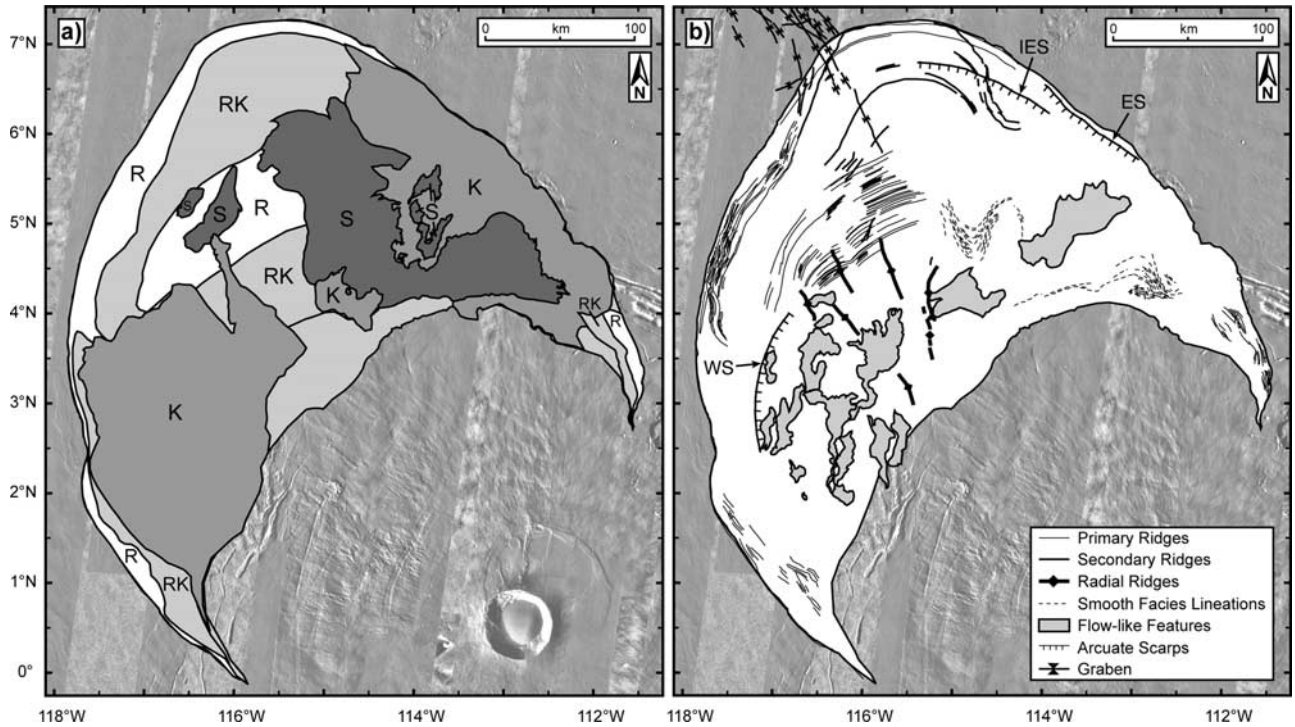

Figure 4. (a) Geologic map of Pavonis Mons fan-shaped deposit showing the location and extent of the characteristic units: ridged (R), knobby (K), smooth (S), and a transitional ridged/knobby facies (RK). The ridged facies at Pavonis Mons consists of tens to hundreds of parallel ridges, concentric to the margins of the deposit, interpreted here as drop moraines produced around the margins of a retreating cold-based glacier. The knobby facies consists of kilometer- to subkilometer-scale hills and hummocks that we have interpreted as sublimation till produced by down-wasting of stagnant, debris-rich ice. The transitional ridged/knobby facies contains sections of the ridged facies superposed by the knobby facies. Finally, the smooth facies consists of broad, smooth plains that we have interpreted as remnant ice from the last phase of glaciation at Pavonis Mons. (b) Geologic map of features within the Pavonis Mons fan-shaped deposit, including primary ridges (thin, solid lines), secondary ridges (thick, solid lines), radial ridges (thick, solid lines with diamonds), smooth facies lineations (thin, dashed lines), graben (thick, solid lines with inward facing triangles), arcuate scarps (solid lines with tick marks, labeled as eastern scarp (ES), inner eastern scarp (IES), western scarp (WS)), and lobate flow-like features (shaded regions). See inset key for clarification. Primary ridges are concentric to the margins of the deposit and make up the ridged facies. Secondary ridges crosscut the primary ridges and are concentric to the margins of the smooth facies, suggesting they were produced by a larger smooth facies during retreat. Radial ridges are radial to the base of the shield and display a unique morphology similar to terrestrial dikes. Smooth facies lineations consist of low-albedo lineations within the smooth facies that outline regions that appear lobate in MOLA topography, suggesting glacial flow has occurred within the smooth facies. The lobate flow-like features consist of unique, steep-sided, leveed flows that appear to originate from a series of fissures on the lower western flanks of Pavonis Mons. The arcuate scarps are large, inward facing scarps, concentric to the margins of the deposit, apparently formed by interactions between lava flows and glacial ice. Several shallow graben are also present in the northwestern regions of the Pavonis deposit, concentric to the margins of the broad, topographic rise to the west.

around 120–130 km, is observed beneath the knobby facies in the western regions of the fan-shaped deposit, approximately 30–50 km from the western margin of the deposit. Depositional features within the Pavonis fan-shaped deposit appear continuous over all three arcuate scarps.

[19] The distal margins of the fan-shaped deposit at Pavonis Mons are well defined due to the morphological contrast between the units of the deposit and the surrounding Tharsis lava plains. However, the proximal boundary of the fan-shaped deposit on the flanks of Pavonis Mons is less distinct. A 100 m high sinuous ridge is observed 50 km from the base of the shield on the northern flanks, and it appears that depositional features may be present for an additional ~50 km up the flanks in these regions.

[20] The Pavonis deposit shares many commonalities with the fan-shaped deposit of Arsia Mons (Figure 2), including each of the three characteristic facies (ridged, knobby and smooth facies) [*Head and Marchant*, 2003]; however, several unique features indicate that additional processes were involved during its formation.

3.1. Ridged Facies

[21] The ridged facies (Figure 4) is most pronounced around the distal margins of the Pavonis deposit; however,

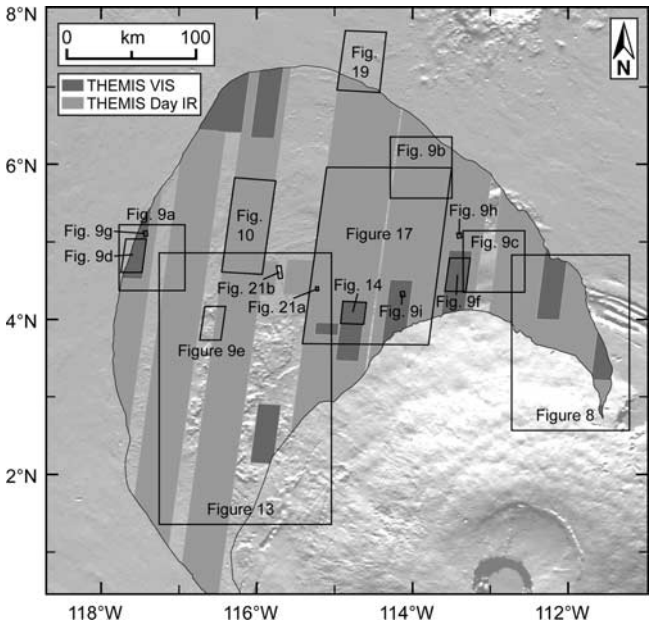

Figure 5. Context map for figure locations on MOLA shaded relief basemap. Solid black lines outline the location of individual figures. Light and dark regions represent THEMIS daytime IR (~73% of Pavonis deposit) and VIS (~15% of Pavonis deposit) coverage, respectively, as of April 2004.

at least 50 ridges are also present in the central, more proximal regions of the deposit. In general, the ridged facies consists of an assemblage of parallel, concentric ridges interspersed in places with small hills [*Scott et al.*, 1998] (Figures 9a–9c). A large 50–100 m high, 1–3 km wide ridge defines the outer margins of the deposit (Figure 9a) while two additional 50–80 m high, 1–2 km wide ridges lie concentric and approximately 10 km inside of this large outer ridge in the northern regions of the deposit (Figure 4). These three large outer ridges appear to have a slightly peaked cross section, although in some areas they appear more rounded and may represent compilations of multiple, closely spaced ridges which appear as one larger ridge at lower resolutions. They also display features indicating that modification has taken place since their deposition, and in places they are broken into a series of smaller sections and hills (Figure 9b). Inside of these large outer ridges, >100, concentric, 5–50 m high and 200–1100 m wide inner ridges are observed (Figures 4, 9a–9c, 10, and 11). The spacing between these inner ridges is variable, with a range of approximately 0.5–4.5 km and their cross-sectional shapes are usually peaked or rounded (Figure 11). The most prominent inner ridges are present in the central regions of the fan-shaped deposit, between 70–130 km from the base of the shield (Figures 4 and 10). The presence of the ridged facies in the central regions of the deposit is unique to the Pavonis fan-shaped deposit, although the ridged facies does appear to continue toward the central regions of the Arsia Mons deposit beneath the knobby facies [*Head and Marchant*, 2003]. The ridges are superposed on underlying topography without significant modification, and do not appear to be deflected by obstacles or depressions. This observation is consistent with the ridged facies of the Arsia fan-shaped deposit where members of the ridged facies are draped over a large impact crater and ejecta blanket with no apparent deflection [*Carr et al.*, 1977; *Williams*, 1978; *Lucchitta*, 1981; *Grizzaffi and Schultz*, 1989; *Anguita and Moreno*, 1992; *Zimbelman and Edgett*, 1992; *Scott and Zimbelman*, 1995; *Helgason*, 1999; *Head and Marchant*, 2003]. This relationship with the underlying terrain suggests that the ridged facies of the fan-shaped deposits was emplaced through a process that involved little interaction with the substrate [*Head and Marchant*, 2003].

[22] On the basis of their morphology and superposition relationships, we interpret these ridges as drop moraines formed at the margins of a retreating cold-based glacier, similar to those observed at Arsia Mons [*Head and Marchant*, 2003]. These moraines are commonly associated with terrestrial cold-based glaciers, such as those observed in the Dry Valleys of Antarctica (Figure 12a) [*Rains and Shaw*, 1981; *Head and Marchant*, 2003]. The formative process for drop moraines involves an equilibrated or retreating cold-based glacier that is experiencing internal flow, bringing supraglacial and englacial debris to the glacier margin. The source of debris for these moraines is typically derived supraglacially within the accumulation zone as opposed to material stripped subglacially from the bed. With time, this debris is transported downglacier and passively deposited at distal margins, forming drop moraines where the glacier margin remains stationary for an extended period of time. The alternating spaces between ridges at Pavonis most likely represent periods of relatively rapid retreat with little deposition separating periods of equilibrium-induced ridge formation. Alternatively, though less likely, the spacing could reflect variable debris content within the glacial ice. The fact that these ridges are present in the central regions of the fan-shaped deposit suggests that

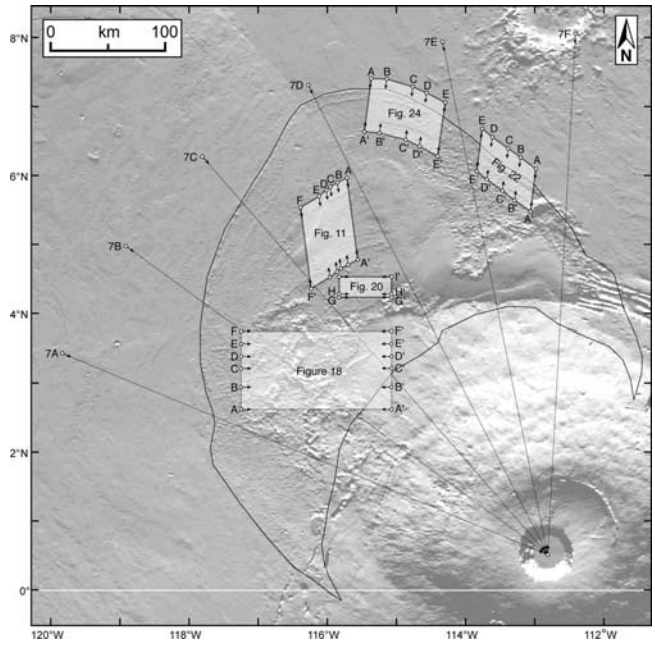

Figure 6. Context map for MOLA profiles on shaded relief basemap. Profiles are grouped by their respective figure numbers with letters representing the locations of individual profiles.

at least one major phase of retreat and deposition by a cold-based glacier occurred, depositing the ridged facies to within 70 km of the base of the shield.

[23] In this model, the large outer ridge represents a moraine that was built up during a relatively long period

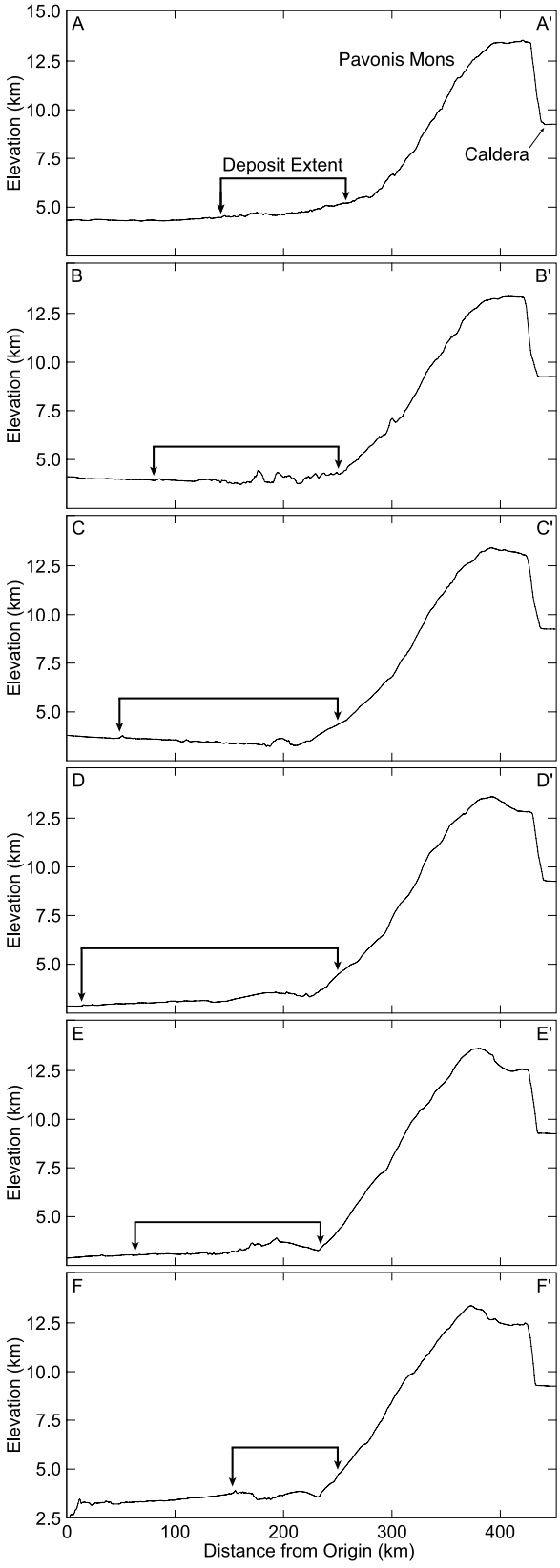

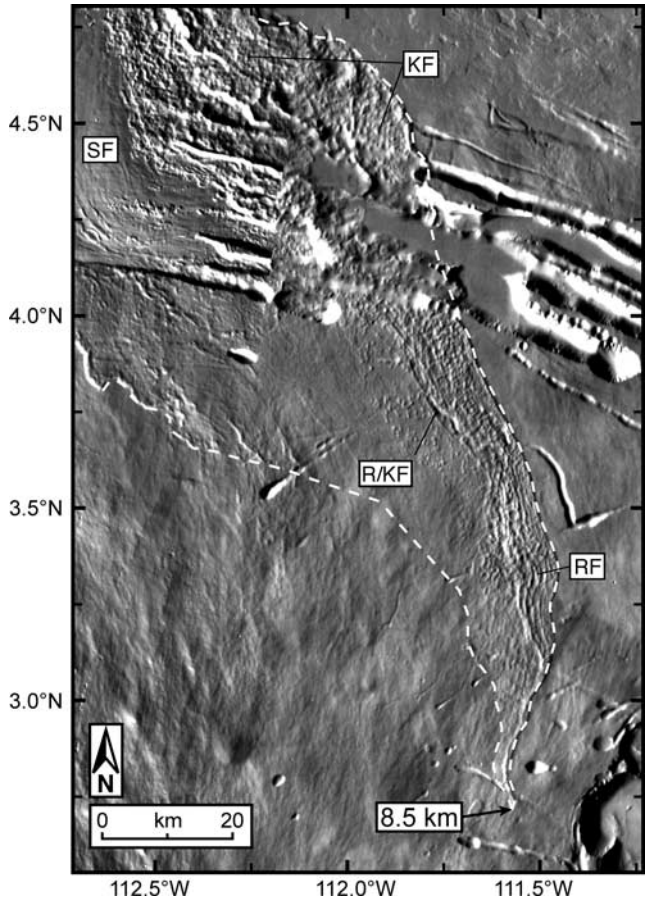

Figure 8. THEMIS daytime IR mosaic of Pavonis Mons northern flank showing the northeastern "horn" of the fan-shaped deposit outlined by the dashed white line. The deposit attains elevations of 8.5 km in these regions and is draped over *Pavonis Fossae*, a series of large graben within the northern flank vent flows. The characteristic facies are present in this image with the ridged facies (RF) around the margins of the deposit, the transitional ridged/knobby facies inward of the ridged facies (R/KF), the knobby facies (KF) in several locations, and the smooth facies (SF) in the northwestern corner of the image.

of glacial stability, followed by a period of retreat with little deposition before forming the other two large outer ridges in a similar manner. The more numerous inner ridges would then be the result of episodes of retreat, stability and

Figure 7. MOLA profiles extracted from 128 pixel/degree gridded MOLA data for Pavonis Mons and associated fan-shaped deposit. Refer to Figure 6 for profile locations. In each profile the thick black bar with arrows delineates the extent of the Pavonis fan-shaped deposit. Profile D-D′ was taken approximately along the axis of maximum elongation for the Pavonis deposit. The deposit is approximately 250 km wide at this location. The topography of the western topographic rise is apparent in profile C-C′ where the terrain west of Pavonis Mons slopes to the east in contrast to regional slopes to the northwest. Vertical exaggeration is 18X.

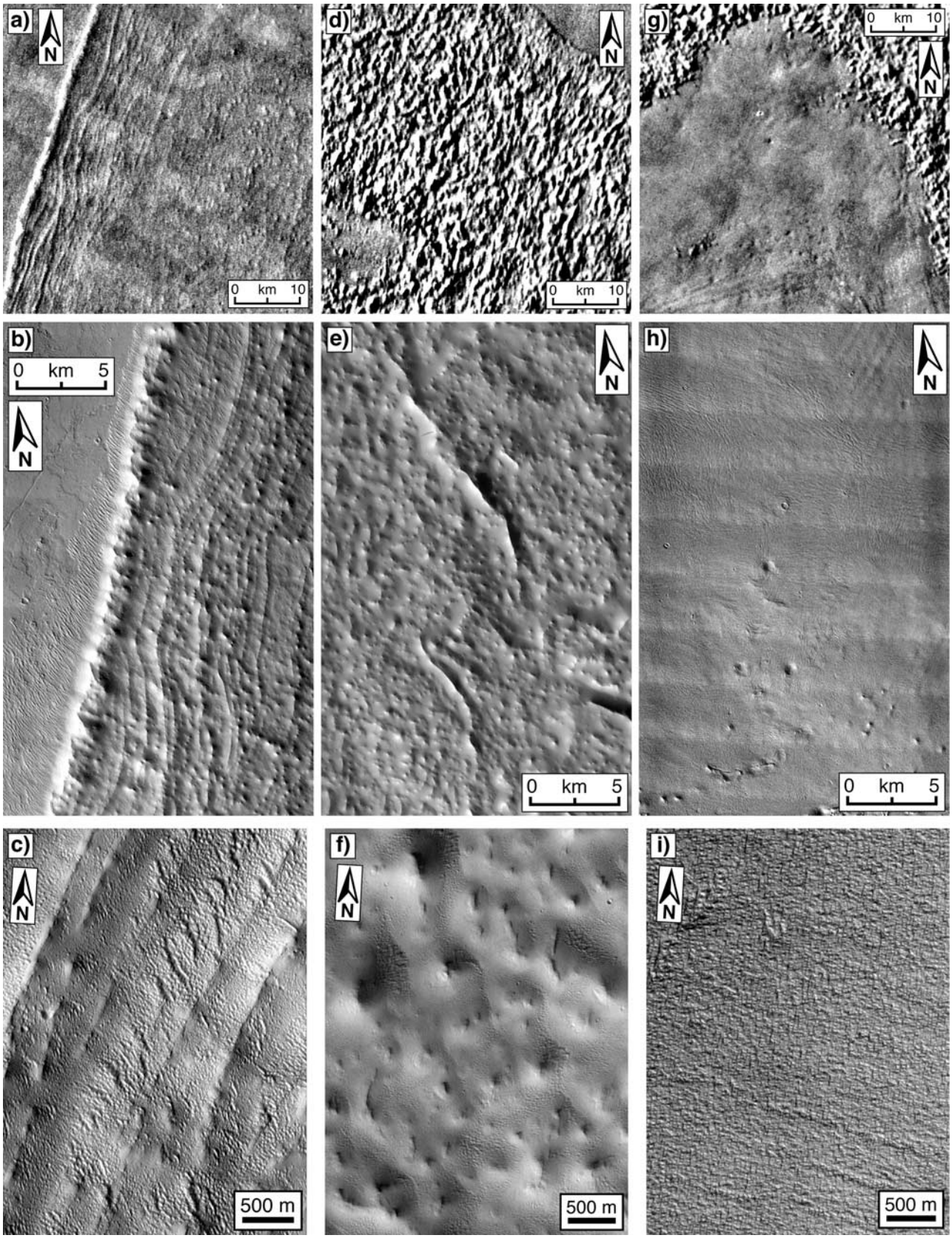
a)
N
0 km 10
d)
N
0 km 10
g)
0 km 10
N
b)
0 km 5
N
e)
N
0 km 5
h)
N
0 km 5
c)
N
500 m
f)
N
500 m
i)
N
500 m

Figure 9

deposition on a smaller scale during a time when the glacier was in an overall state of retreat. The ridges at Pavonis are at various stages of preservation, and in general, the ridges closer to the margins of the deposit appear to have experienced more modification (Figure 9b) than the well-preserved, inner ridges in the central regions of the deposit (Figure 10). This suggests that the inner ridges are younger than the outer ridges or may have been shielded from erosional processes until relatively recently. Alternatively, the apparent disparity in erosional rates may indicate that the large outer ridges were previously ice-cored or currently contain a significant ice component. This ice-cored hypothesis is consistent with the high relief and apparent volume of the larger members of the ridged facies. Analysis of terrestrial drop moraines reveals that they can often contain a significant ice component preserved beneath the overlying debris cover [e.g., *Rains and Shaw*, 1981; *Benn and Evans*, 1998], and this might be even more pronounced on Mars.

3.2. Knobby Facies

[24] The knobby facies at Pavonis (Figure 4) consists of collections of subkilometer- to kilometer-scale, circular to elongate hills and mounds which appear to collectively form arcuate lineations in places (Figures 9d–9f) [*Scott and Zimbelman*, 1995; *Scott et al.*, 1998; *Head and Marchant*, 2003]. The knobby facies at Pavonis superposes underlying members of the ridged facies (e.g., Figure 10), similar to the knobby facies at Arsia [*Head and Marchant*, 2003]. However, the unit contacts between the Pavonis knobby and ridged facies are not as clearly defined as those for the Arsia deposit; in many places, a gradational relationship exists between the ridged facies and knobby facies that was mapped as a transitional ''ridged and knobby unit'' by *Zimbelman and Edgett* [1992]. We have included this unit in our geologic map of the Pavonis deposit for areas containing members of the ridged facies and sparsely distributed concentrations of the knobby facies (Figure 4). *Scott et al.* [1998] noted that small hills in the ridged facies grade into the knobby facies in places within the Pavonis deposit, but more commonly a noticeable increase in hill size occurs at their common boundary. We have used this relationship to define the boundaries of the knobby facies in our geologic map (Figure 4). The spatial density and distribution of the Pavonis knobby facies is variable, with relatively homogeneous distribution in the northeastern and western regions of the deposit, and patchy distribution in the northwestern and central regions (Figure 4). Certain concentrations of the knobby facies in the northern regions of the Pavonis fan-shaped deposit appear elongated in plan view (Figure 10), and have been interpreted as drumlin fields or drift deposits produced during subice disintegration [*Scott et al.*, 1998]. In addition, *Scott et al.* [1998] interpreted streamlined, coalesced groups of hills as eskers within these drumlin-like fields. Drumlins and eskers are typically associated with basal meltwater activity beneath wet-based glaciers; however, we have found no additional evidence suggesting wet-based activity in these regions of the Pavonis deposit.

[25] It has also been suggested that the hills of the knobby facies may be aligned hummocks on a lava or debris flow [*Scott et al.*, 1998], or possibly wind-faceted yardangs in friable materials, resulting from downslope winds originating at the summit of Pavonis Mons [*Scott et al.*, 1998]. Conversely, the knobby facies appears to be a mantling deposit and is not confined to one particular underlying unit such as a highly eroded lava flow. The knobby facies also appears to continue uninterrupted onto lobate, volcanic flow-like features (Figures 9e and 13) that have a relief of several hundred meters above the surrounding deposit. Furthermore, the knobs and hills do not display a preferred orientation, and they appear more circular in shape in the regions closest to the shield, arguing against a yardang origin.

[26] High-resolution MOC narrow-angle images and THEMIS VIS images of the smooth facies reveal a zone

Figure 9. Characteristic images of the three main facies within the Pavonis fan-shaped deposit at Viking resolution (a, d, g, 50–200 meters/pixel), THEMIS VIS resolution (b, e, h, 19 m/pixel), and MOC narrow-angle resolution (c, f, i, 5–6 m/pixel). Refer to Figure 5 for context information. (a) Viking image of ridged facies along the western margin of the Pavonis deposit. Note the size of the large outer ridge and relationship with smaller inner ridges. (b) THEMIS VIS image of the ridged facies along the northwestern margin of the deposit (Image V07731018). Image covers a section of the Viking image in Figure 9a, clearly displaying the enhanced resolution of THEMIS VIS images. Note the lava flow texture to the west of the deposit, the large outermost ridge, and smaller inner ridges, interpreted to be drop moraines. Some ridges are broken into smaller sections or hills and appear to have undergone additional modification since their deposition. Also note the sinuosity of some ridges toward the edifice and their superposition, suggesting multiple phases of advance and retreat. (c) MOC narrow-angle image of ridges along western edge of the Pavonis deposit (Image M0700568). Notice the presence of dune fields interspersed between the individual ridges, suggesting eolian modification of the ridges has occurred and is currently occurring. (d) Viking image of knobby facies with relatively homogeneous coverage in northeastern region of the Pavonis deposit. (e) THEMIS VIS image of the knobby facies over the western flow-like features (Image V08068017). At this resolution, individual knobs can be distinguished, some appearing more rounded, while others appear more elongated in nature. Large ridges in image are the leveed edges of the lobate flow-like features discussed in section 3.4. (f) MOC narrow-angle image of the knobby facies displaying morphology of individual knobs and interspersed dune fields (Image E1302319). (g) Viking image of the main smooth facies deposit at Pavonis displaying the relationship with the surrounding knobby facies and lineations toward the southern edge of the image. (h) THEMIS VIS image of the main smooth facies deposit at Pavonis (Image V07993021). Notice the undulating texture of the surface, low-albedo lineations in the northern portion of the image, and knobs apparently being exhumed from beneath the smooth facies in the southern portion of the image. Circular depressions within the smooth facies may represent softened impact craters or the influence of underlying members of the knobby facies. (i) MOC narrow-angle image of the smooth facies (Image E1202942). Notice the small-scale undulations on the surface that appear to be dune fields.

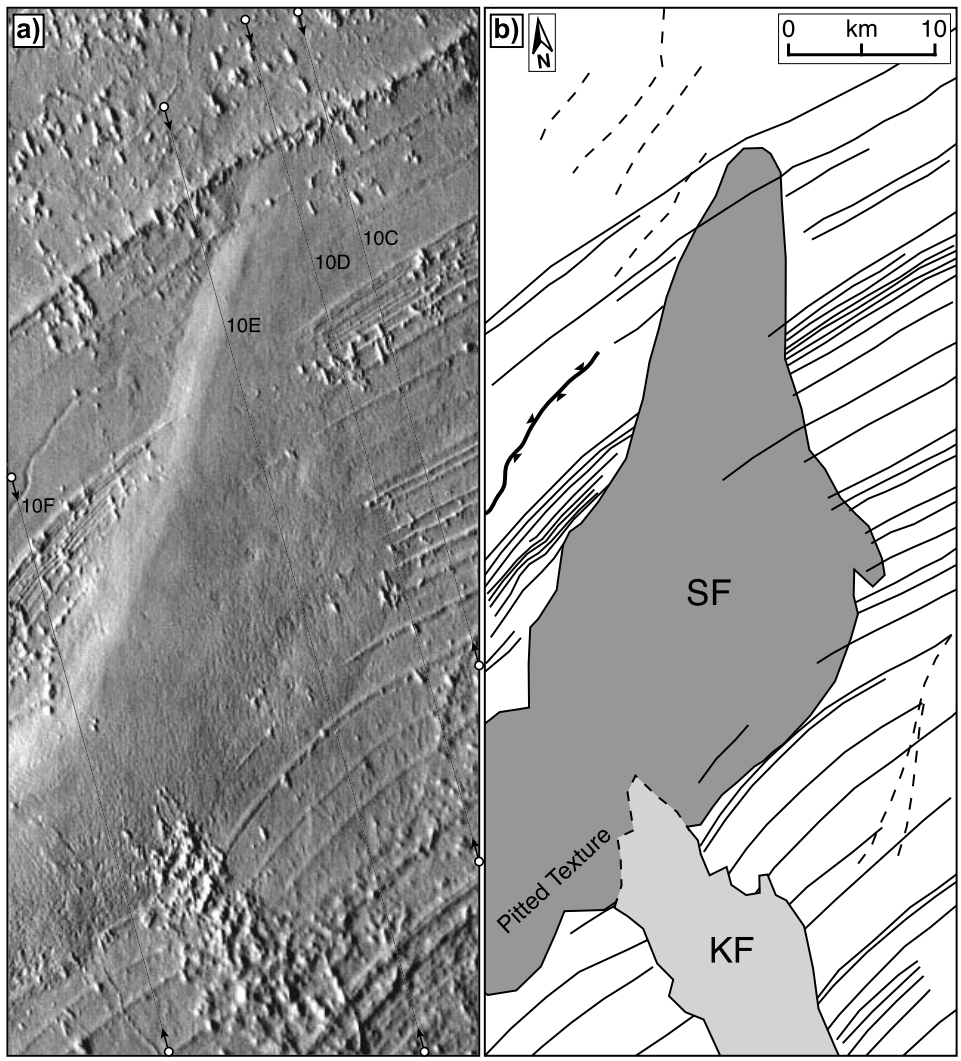

Figure 10. (a) THEMIS daytime IR image of smooth facies inner outlier and central ridges showing the superposition relationship among the three main geologic units of the Pavonis fan-shaped deposit. The ridged facies is present beneath sections of the knobby facies, while the smooth facies is covering both the ridged and knobby facies; some ridges and knobs are visible through the thinner margins of the smooth facies. The thin, southeastern margin of the smooth facies outlier in this figure appears rougher and pitted when compared to the thicker central regions. Some individual knobs in these regions of the Pavonis fan-shaped deposit (upper part of the image) appear elongated with a NW-SE major axis orientation and have been interpreted as drumlins in the past [*Scott et al.*, 1998]. The thin solid lines with arrows at endpoints specify the location of MOLA profiles presented in Figure 11 although the actual endpoints of these profiles are beyond the extent of this image. Refer to Figure 6 for full profile context. (b) Sketch map of the image in Figure 10a, highlighting smooth facies (SF, dark gray), knobby facies (KF, light gray), primary ridges (solid lines), and secondary ridges (dashed lines). The thick solid line with inward pointing triangles represents a channel to the northwest of the inner outlier that may be related to localized meltwater activity.

of "fresh" or less-modified knobby terrain that is present around some of the margins of the smooth facies (Figure 14). This "fresh" zone is typically around 5–10 km wide and is characterized by sharper, well-defined peaks and ridges with less eolian modification and noticeably fewer dunes between topographic highs. In contrast, the morphology of the terrain at greater distances than this 5–10 km wide zone is typical of the knobby facies with more rounded hills, shallower slopes and infilling between knobs (Figure 14).

[27] The distribution of the knobby facies is anisotropic in the central regions of the Pavonis fan-shaped deposit as well as in close proximity to the lobate flow-like features in the western regions of the deposit (Figure 13). For example, a concentration of the knobby facies is present on the western side of a radial ridge in the central regions of the deposit, while the eastern side of the ridge is almost entirely free of any knobs or hills (Figure 13). In addition, a concentration of the knobby facies is present approximately 20 km east of this radial ridge (Figures 10 and 13). Some of the inner

ridges also form an indentation directed toward the shield in the shape of a "v" that appears to be centered around this concentration of the knobby facies, while the topography does not show any significant variation (Figures 10 and 13).

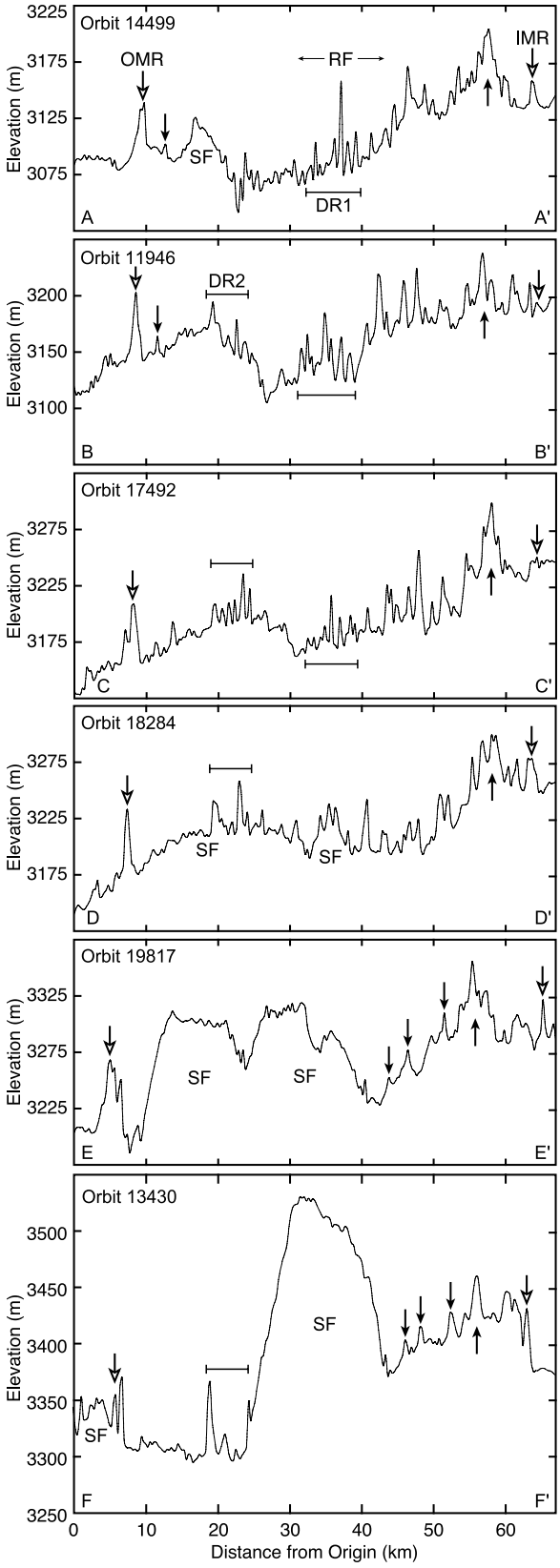

There are also a few regions between the western lobate features where the knobby facies is sparse or absent, while it is present on the surrounding flows (Figure 13).

[28] In summary, the knobby facies of the Pavonis fan-shaped deposit (1) consists of kilometer- to subkilometer-scale irregular hills and valleys, (2) appears passively deposited over underlying topography, (3) is superposed on the ridged facies, and (4) displays localized anisotropic distribution throughout the fan-shaped deposit. We interpret the knobby facies as a sublimation till derived from in situ down-wasting of ash- and debris-rich glacier ice, similar to the well-documented sublimation tills in terrestrial glacial environments such as the Antarctic Dry Valleys (Figure 12b) [e.g., *Benn and Evans*, 1998; *Marchant et al.*, 2002; *Head and Marchant*, 2003]. A sublimation till forms when debris-laden ice experiences sublimation while any englacial and supraglacial debris contributes to a growing supraglacial lag deposit. This lag deposit will continue to grow until the underlying ice has completely sublimated or the debris cover is thick enough to significantly retard ice sublimation.

[29] One form of terrestrial till produces large, circular mounds of ice and debris known as dirt cones. While terrestrial dirt cones have been documented as features commonly associated with meltwater activity [*Lewis*, 1940; *Swithinbank*, 1950; *Benn and Evans*, 1998], the underlying principles for formation are present in situations where ablation occurs predominantly through sublimation. The formative mechanism for these features is differential ablation on the surface of a glacier where the debris cover is thinnest, while thicker debris cover in surrounding areas tends to preserve underlying ice [*Lewis*, 1940; *Swithinbank*, 1950; *Benn and Evans*, 1998]. As more ice is lost beneath the thin debris cover, the slope between these two areas steadily increases until the thick debris cover slides, exposing the preserved ice [*Swithinbank*, 1950]. This newly exposed ice then begins to ablate, while the area previously undergoing ablation is preserved under a thicker debris cover. This process often undergoes several cycles until the debris cover is sufficiently thick to hinder further ablation, resulting in collections of roughly circular, debris-covered, ice-cored mounds. These features often form in crevasses or other depressions on the surface of a glacier that serve as a sink for atmospherically deposited debris [*Lewis*, 1940; *Swithinbank*, 1950]. Some terrestrial dirt cones have been documented with heights of >30 m [*Swithinbank*, 1950] and they can form linear sequences. This process may account for the observation that some

Figure 11. MOLA profiles of the central ridges at Pavonis. Refer to Figures 6 and 10 for profile context. In each profile, the larger arrows with white fill represent the outermost (OMR) and innermost (IMR) ridges of the central ridges. Many smaller, 5–50 m high ridges can be delineated in each profile between these two outermost ridges. The smaller arrows represent features that can be identified in adjacent profiles. The bars labeled DR1 and DR2 highlight dense collections of the central ridges with less spacing between ridges. The inner outlier of the smooth facies (labeled SF) is present in profiles D-D′, E-E′, and F-F′. Vertical exaggeration is 158X.

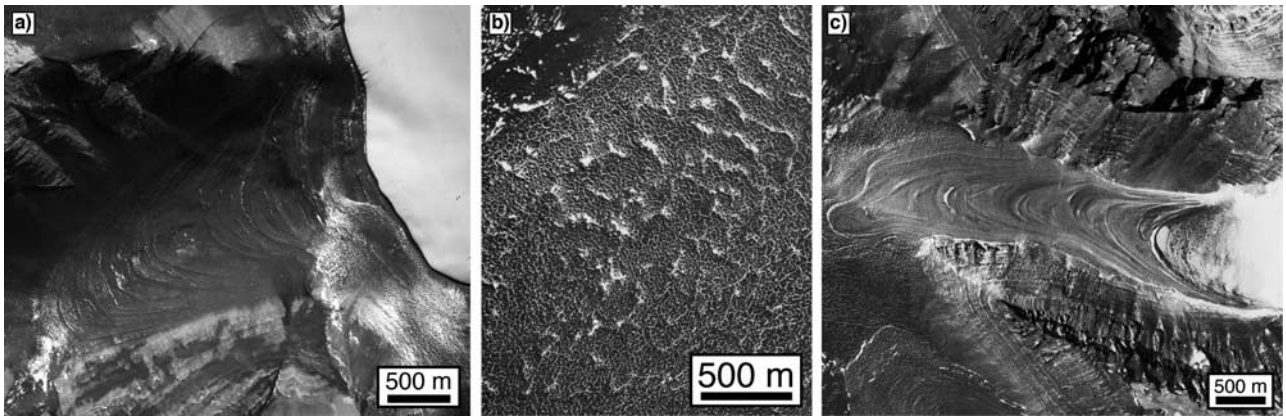

Figure 12. Terrestrial analogs for the Pavonis fan-shaped deposit in the Dry Valleys of Antarctica: (a) drop moraines in Arena Valley as a terrestrial analog for the ridged facies (U.S. Geological Survey aerial photograph TMA 3079/303, taken 21 November 1993), (b) sublimation till in Beacon Valley as an analog for the knobby facies (U.S. Geological Survey aerial photograph TMA 3078/006, taken 21 November 1993), and (c) debris-covered rock glacier in Mullins Valley as a possible analog for localized flow within the smooth facies (U.S. Geological Survey aerial photograph TMA 3080/275, taken 21 November 1993). See color version of this figure in the HTML.

members of the knobby facies appear to have a linear or elongated orientation.

[30] The uneven spatial distribution of the knobby facies at Pavonis indicates that the debris distribution over the glacier was anisotropic at the time of deposition. For instance, the unusual concentrations of the knobby facies adjacent to the western flow-like features (Figures 10 and 13) may represent the location of topographic lows on the glacial surface or the former conjunction between two glacial lobes, where we would expect to see greater accumulation of debris.

[31] The knobby facies may also represent another class of terrestrial glacial features known as "ribbed" or "Rogen" moraines [*Scott and Zimbelman*, 1995]. These features are typically found covering large areas where the interior portions of the Laurentide and Scandinavian ice sheets once existed [*Clark and Meehan*, 2001]. They consist of numerous, closely spaced "ridges," which are formed transverse and, less often, parallel to ice flow in a subglacial position with a straight to arcuate planform. These ribbed moraines also display a consistent size, strong regularity in spacing, occurrence of anastomosing ridges, downstream pointing "horns," and irregular bumps in elevation along ridge crests [*Clark and Meehan*, 2001]. Terrestrial ribbed moraines have been documented with similar dimensions to the hummocks in the knobby facies. One model for their formation involves deformation of debris-rich ice, suggesting that "Rogen moraine is composed of thrust slices of basal ice, stacked up by compressive flow beneath the glacier" [*Bouchard*, 1989; *Benn and Evans*, 1998]. "Such thrusting is thought to occur in topographic hollows where ice flows against obstacles on the bed, or at junctions between warm-based, sliding ice located upglacier and cold-based ice downglacier" [*Benn and Evans*, 1998]. These features are not yet well understood, and they may also be the result of bed deformation by sliding ice, which would effectively erase any previous glacial debris landforms. If this is the case, then this explanation cannot account for the Pavonis knobby facies due to its relationship with the well-preserved ridged facies. However, the ribbed moraine hypothesis should not be ruled out as a formative mechanism for the knobby facies until additional data can be collected both on Mars and Earth.

[32] The observation that the knobby facies of the Pavonis fan-shaped deposit is not uniformly distributed as it is at Arsia [*Head and Marchant*, 2003] indicates that it may have had a somewhat different formative history. The presence of the knobby facies and its superposition on the ridged facies (Figure 10) indicate that there was an additional phase of glacial advance after the previous phase of retreat and deposition to form the ridged facies. If the knobby facies formed through sublimation of debris-rich ice, the conditions at the time of emplacement were undoubtedly different from the conditions during deposition of the ridged facies. Instead of a slow, intermittent lateral retreat, our model suggests that the knobby facies was deposited during sublimation and down-wasting of the ice with lateral movement or internal ice deformation playing a secondary role. This suggests that during emplacement of the ridged facies, conditions were fairly stable with short-term cycles of stagnation, retreat, and deposition to form ridges with a relatively regular spacing. During deposition of the knobby facies, climatic conditions likely shifted from a period of extended stability to an environment favoring increased sublimation, down-wasting, and the resultant sublimation till instead of drop moraines.

3.3. Smooth Facies

[33] The smooth facies of the Pavonis fan-shaped deposit covers an area of approximately 12,500 km^2 (Figure 4) and is superposed on all other units of the deposit without disrupting underlying features (Figure 10). There are four main regions of the smooth facies (Figure 15); the largest of which covers an area of 11,000 km^2 in the central regions of the fan-shaped deposit and is referred to here as the main smooth facies deposit (Table 2). The smooth facies generally has gentle slopes of around 0.5–1.5°; however, some of the outer margins of the smooth facies (e.g., the 60–70 km long western margin of the main smooth deposit) have much steeper slopes of around 3–5° (Figures 15 and 16). THEMIS daytime IR and VIS images reveal circular

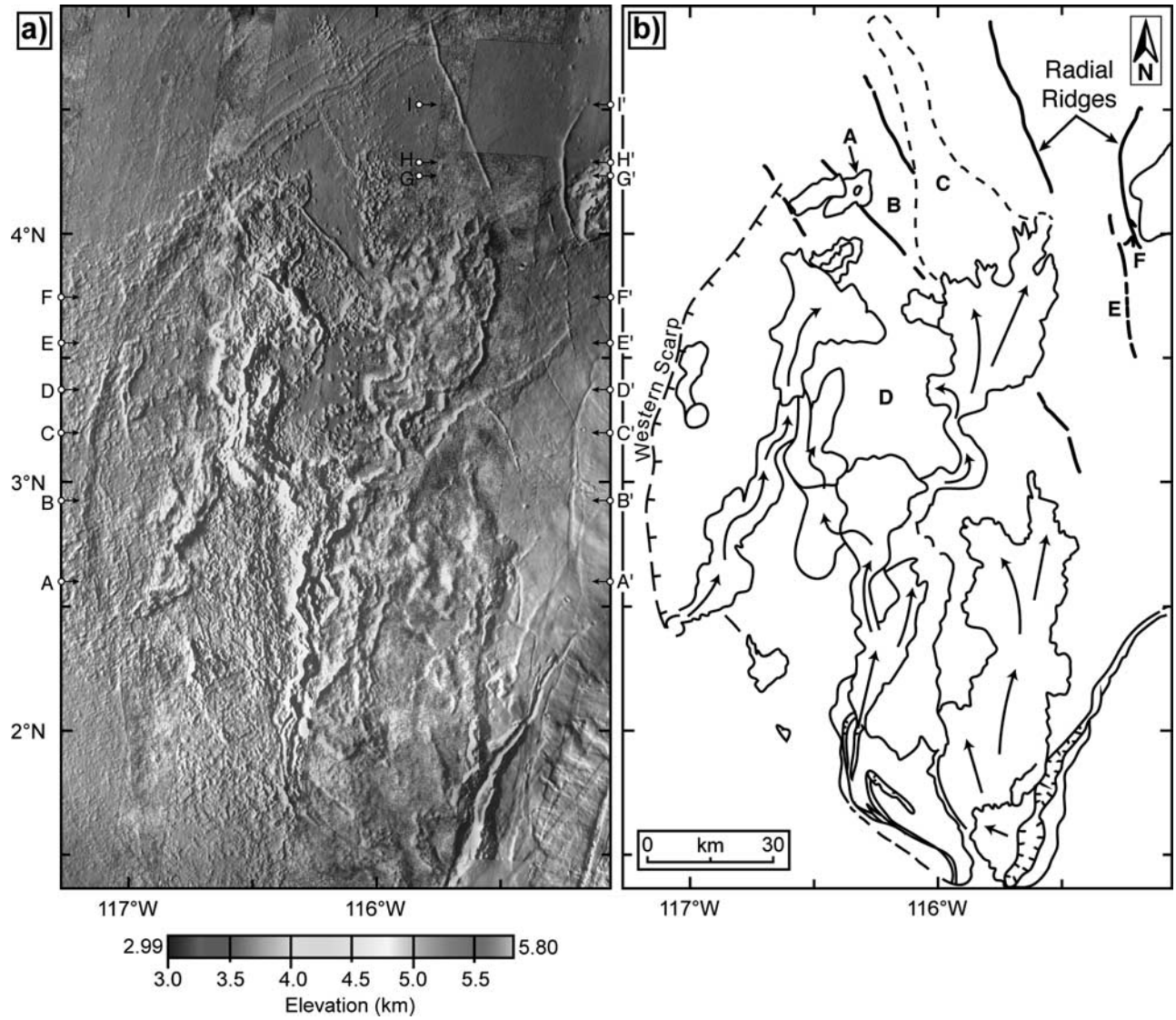

Figure 13. (a) Mosaic of THEMIS daytime IR and Viking data with MOLA color overlay of the western lobate flow-like features, radial ridges, western arcuate scarp, and superposed knobby facies. Circles with arrows represent the endpoints of the MOLA profiles across the flow-like features in Figure 18 (A–F) and across the radial ridges in Figure 20 (G–I). (b) Sketch map. Flow-like features are outlined with apparent direction of flow shown by arrows. These features are interpreted as highly silicic lava flows emanating from vents on the western flank of Pavonis Mons or as potential subglacial flows. Radial ridges, interpreted as dikes possibly erupted in a subglacial environment, are mapped as thick solid lines. One radial ridge appears to expand into a pancake-like feature that we have interpreted as a possible subglacial sill (A). Other ridges appear en echelon (E) or forked (F) in places. The western scarp is mapped by the dashed line with tick marks. The distribution of the knobby facies is anisotropic in these regions. A concentration of the knobby facies is present on the western side of a radial ridge, while the eastern side of the ridge is almost entirely free of any knobs or hills (B). In addition, a dense concentration of the knobby facies is present approximately 20 km east of this radial ridge (C). There are also regions between the western lobate features where the knobby facies is sparse or absent (D), while it is present on the surrounding flows. See color version of this figure in the HTML.

depressions within the smooth facies that may be attributed to underlying members of the knobby facies or impact cratering (Figures 9g and 9h). These features are generally less than a few kilometers in diameter and appear degraded or softened.

[34] MOC images across the smooth facies show undulations on the surface of the smooth facies that appear to be dune fields (Figure 9i). These dunes are typically a few meters high and 30–100 m wide, with a spacing of around 50–100 m. In general, the dunes in the thicker, central regions of the deposit appear smaller, generally on the order of a few meters, while the dunes covering the thinner margins are larger, some appearing to reach heights of up to 25 m based on MOC narrow-angle shadow measure-

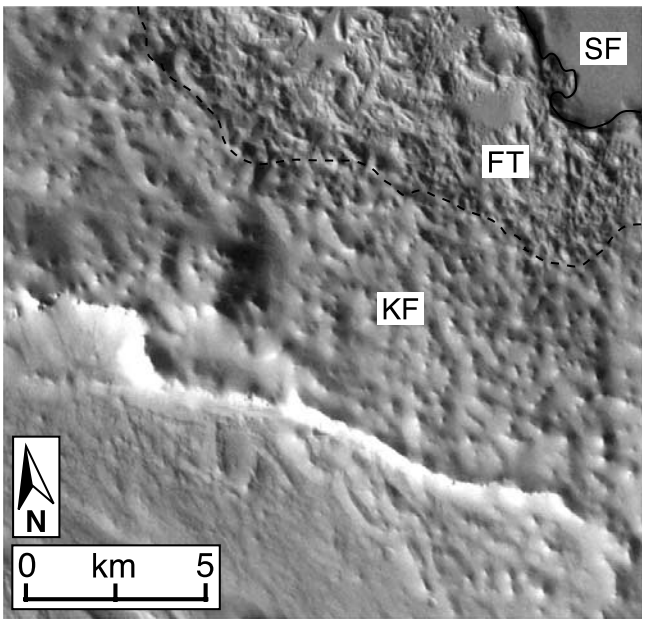

Figure 14. THEMIS VIS image showing the "fresh" knobby terrain surrounding the margins of the smooth facies (Image V07656019). The smooth facies (SF) is present in the northeastern corner of the image, the zone of "fresh" terrain (FT) is approximately 5–10 km from the margins of the smooth facies, and the more characteristic knobby facies (KF) is present to the southwest of the "fresh" terrain. The black dashed line represents the approximate boundary between the zone of "fresh" terrain and the knobby facies. The large ridge within the knobby facies is the leveed edge of one of the lobate flow-like features.

ments. The margins of the smooth terrain also appear more highly degraded with a pitted appearance in places (Figure 10).

[35] The smooth facies at Pavonis bears some resemblance to the smooth, arcuately lineated material of the Arsia Mons fan-shaped deposit [*Zimbelman and Edgett*, 1992; *Scott et al.*, 1998]. However, low-albedo, closely spaced, concentric lineations within the Pavonis smooth facies (Figures 9h, 15, 16, and 17) are not as common as those associated with members of the smooth facies at Arsia, which have been interpreted as debris-covered rock glaciers [*Lucchitta*, 1981; *Head and Marchant*, 2003]. The lineations within the Pavonis smooth facies are limited to the main deposit and are more pronounced closer to the base of the shield (Figures 15 and 17). These lineations outline regions within the smooth facies that appear lobate in MOLA topography data (Figure 15).

[36] There are two smaller isolated outliers of the smooth facies approximately 40 and 60 km to the west of the main smooth facies deposit (Figures 10 and 15). A fourth isolated outlier, which we have classified as the "mountain outlier" (based on terminology of *Zimbelman and Edgett* [1992]), is present beyond a series of elevated peaks to the northeast of the main smooth deposit (Figures 15 and 17). In addition, there are isolated patches of the smooth facies within the knobby facies to the east of the main smooth facies deposit (Figures 15 and 17). Quantitative data for each of the four major regions of the smooth facies are available in Table 2.

[37] On the basis of superposition relationships, it has been suggested that the smooth facies may consist of pyroclastic flows, ash-flow tuffs, or lahars that erupted from volcanic vents after the emplacement of the ridged and knobby facies [*Zimbelman and Edgett*, 1992; *Scott and Zimbelman*, 1995; *Scott et al.*, 1998]. MOLA topography, however, reveals that the smooth terrain does not occupy regions of lower elevation (Figures 15 and 16) the way such flows would be expected to behave. Typical terrestrial pyroclastic flows are characterized by "ponding" in topographic lows and thinning in regions of higher elevation [*Cas and Wright*, 1987]. In contrast, the smooth facies at Pavonis Mons forms convex lobes, some with thicknesses of over 500 m above the surrounding terrain (Figure 15, Table 2). The presence of outliers and isolated patches of the smooth facies can also be interpreted as evidence suggesting that the smooth facies is not the result of one large volcanic event from a single source. Taken together, we believe that these observations require an alternate explanation to the pyroclastic flow origin.

[38] We interpret the smooth facies at Pavonis Mons to be the remnants of a larger, continuous smooth deposit, specifically debris-covered ice that was once part of the most recent glacial activity at Pavonis. This interpretation is supported by MOLA topography data, which clearly show the lobate nature and unusually high relief of the smooth facies (Figures 15 and 16). In addition, lineations within the

Figure 15. (a) MOLA shaded relief map of Pavonis smooth facies with color overlay. The smooth facies appears lobate in nature and approaches thicknesses of over 500 m in the central regions of the main deposit (see Figure 16). Notice the areas of lower topography immediately adjacent to the margins of the smooth facies, suggesting that the smooth facies is not the result of pyroclastic flows as previously proposed by *Scott et al.* [1998]. The eastern scarp and inner eastern scarp are also apparent in the gridded MOLA data. The eastern scarp is over 80 km long with a relief of over 200 m in places and is concentric to the eastern boundary of the fan-shaped deposit. We have interpreted this scarp as the result of lava banking against a glacier early in the history of the Pavonis fan-shaped deposit. The inner eastern scarp is present approximately 20–30 km from the eastern scarp and appears to be the inner margin of a concentric band of material. Circles with arrows represent the endpoints of the MOLA profiles in Figure 16. (b) Sketch map of smooth facies (red), lineations (solid lines within smooth facies), secondary ridges (dashed lines), scarps (solid lines with tick marks), and total coverage of the fan-shaped deposit (yellow). The individual deposits of the smooth facies appear to be the remains of a once-larger, continuous smooth facies deposit. The secondary ridges are not parallel to the concentric ridged facies; instead, they appear concentric to the margins of the smooth facies. These features may represent drop moraines produced during the retreat of the earlier manifestation of the smooth facies. Lineations within the smooth facies appear to define regions where glacial flow was or is currently taking place.

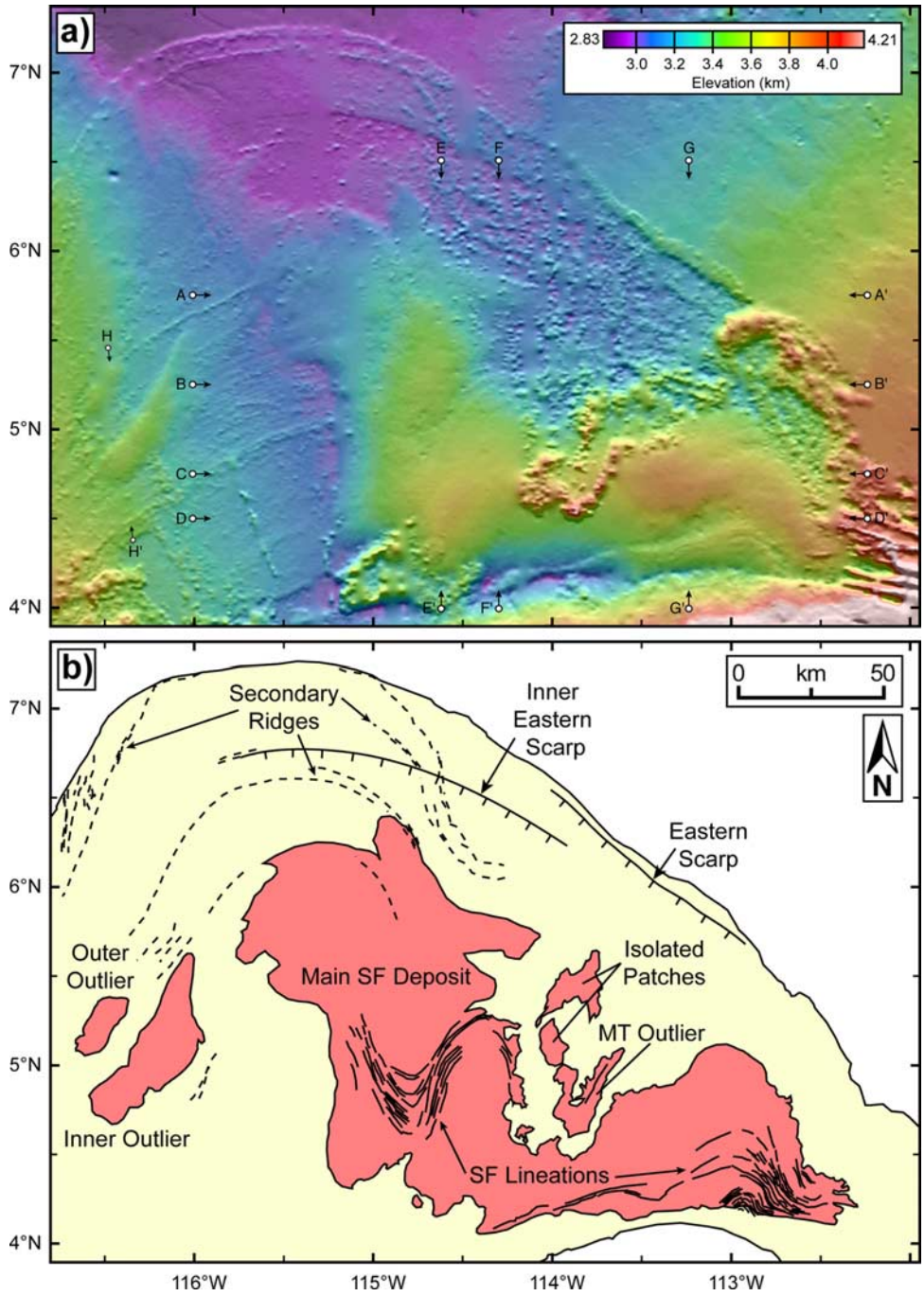

Figure 15

smooth facies (Figures 15 and 17) that appear to define individual lobes within the main deposit may represent regions of the smooth facies that underwent or are currently undergoing rock-glacier-like flow similar to the smooth facies at Arsia Mons (Figure 12c). Finally, the zone of "fresh" knobby facies immediately surrounding the smooth terrain (Figure 14) appears to represent knobby terrain that was preserved beneath a larger smooth facies deposit. As

Table 2. Quantitative Data for the Smooth Facies at Pavonis Mons

Smooth Facies Subunit	Surface Area, km^2	Dimensions: Height × Width, km	Maximum Thickness, m	Maximum Elevation, km
Main Deposit	11,000	140 × 200	~500–600	~3.90
Inner Outlier	822	60 × 20	~250	~3.55
Outer Outlier	184	25 × 10	~150	~3.55
Mountain Outlier	148	30 × 23	~50–100	~3.75

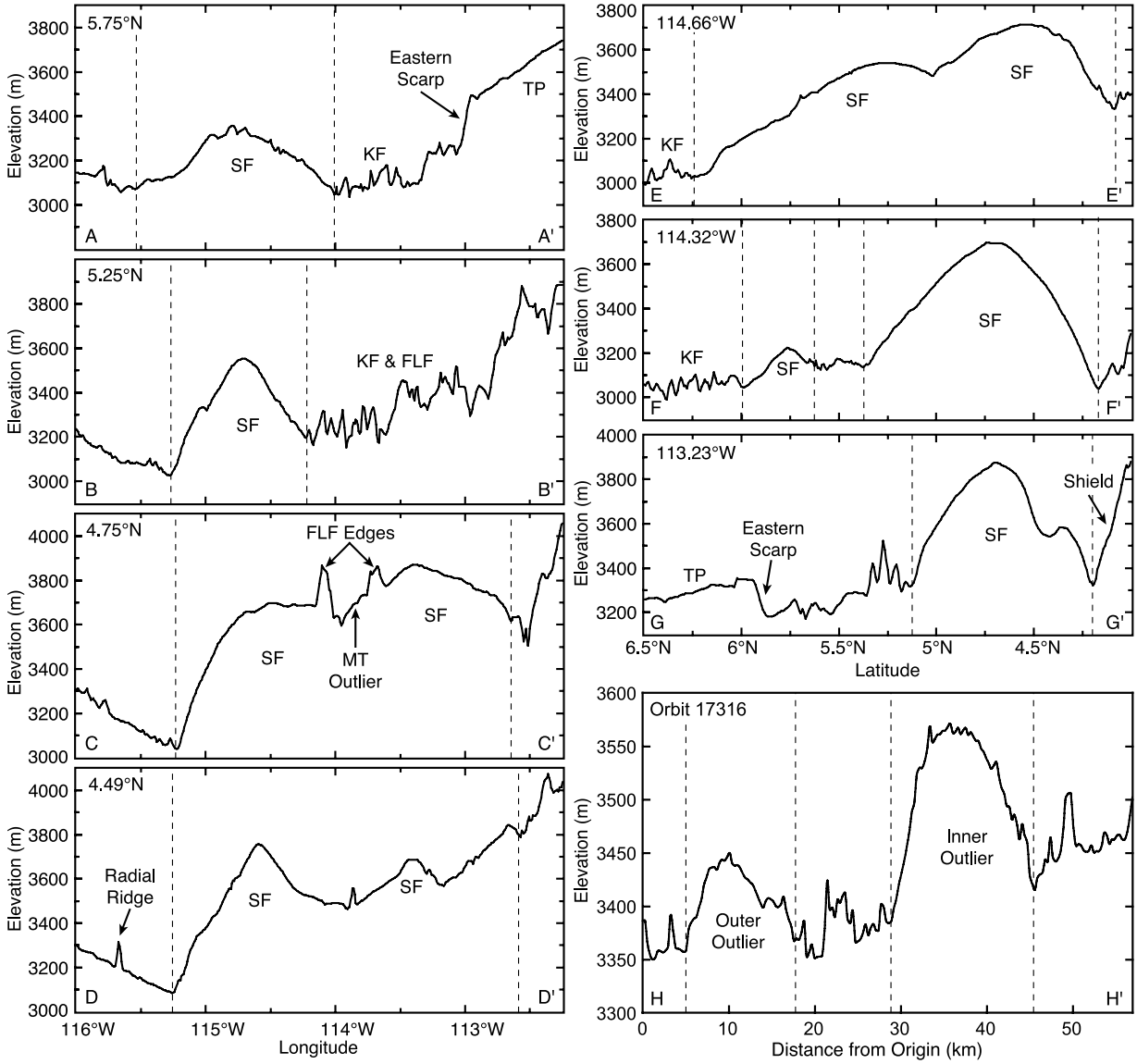

Figure 16. MOLA profiles of smooth facies. Profiles A-G are extracted from 128 pixel/degree gridded MOLA data with a latitudinal orientation (A-D, vertical exaggeration 105X) and a longitudinal orientation (E-G, vertical exaggeration 68X). Profile H was extracted from MOLA orbit 17316 across the inner and outer smooth facies outliers (vertical exaggeration 124X). See Figure 15 for context and location of profiles. Note the lobate nature of the smooth facies in each profile. Profile C-C′ crosses the main smooth facies deposit as well as the MT outlier which is isolated by adjacent topography. Note the steeper western edge of the main smooth facies deposit and eastward slope of the terrain located to the west of the main smooth deposit. This relationship suggests that the smooth facies does not consist of pyroclastic flows. Pyroclastic flows would be expected to occupy regions of lower topography instead of attaining the observed relief. Profile E-E′ shows individual sections of the main smooth facies deposit that appear lobate, while profile F-F′ shows that the smooth facies appears to be over 600 m thick in places. In each profile, knobby facies is labeled KF, flow-like features are labeled FLF, and the Tharsis Plains to the east of the Pavonis fan-shaped deposit are labeled TP.

the once-larger smooth facies deposit continued to retreat and sublimate, new exposures of the underlying knobby facies were exhumed and subjected to erosional modification. Under these circumstances, we would expect to see a transition from the characteristic knobby terrain to less-modified, ''fresh'' knobby terrain with decreasing distance from the margins of the smooth facies. This same process may account for the observed disparity in modification state between the well-preserved central ridges and the modified outer ridges discussed in section 3.1.

[39] Further evidence supporting the presence of a continuous smooth facies with greater coverage in recent history comes from the spatial relationship of the mountain outlier and isolated patches of the smooth facies with the main smooth deposit. The mountain outlier is separated from the main deposit by a continuous topographic barrier

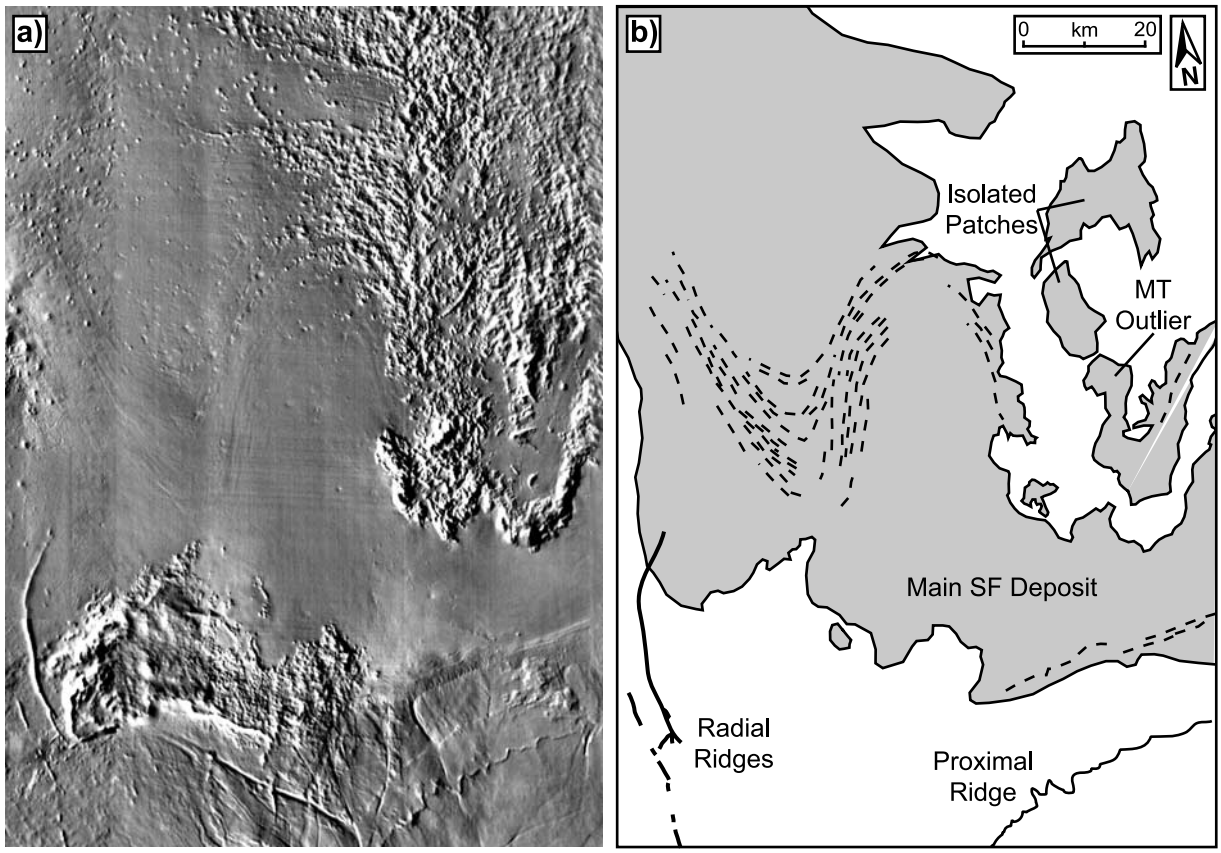

Figure 17. (a) THEMIS daytime IR mosaic of a portion of the main smooth facies deposit. Note the superposition and contrast of the smooth facies and the surrounding knobby facies. Faint low-albedo lineations outline regions of the smooth facies that appear lobate in MOLA data. (b) Sketch map of the area highlighting the smooth facies (shaded), smooth facies lineations (dashed lines), radial ridges (thick solid lines), and proximal ridge (thin solid line in the southeast corner of image) that represents the proximal traces of the Pavonis fan-shaped deposit on the shield. Note the isolated patches of smooth facies and MT outlier that are present within the knobby facies, suggesting a larger, continuous smooth facies existed in the past.

(Figures 15, 16, and 17), and there do not appear to be any low-elevation channels or conduits that would allow for material exchange between the two deposits. If the individual members of the smooth facies were once a continuous glacier that covered this topographic barrier, we would expect that an isolated outlier would be separated from the main deposit during ablation and retreat. The same holds true for the isolated patches of smooth material that fill valleys within the knobby facies, which are clearly separated from the main deposit (Figures 15 and 17).

[40] We also see an additional series of ridges that appear to be superposed on all other units within the Pavonis fan-shaped deposit, excluding the smooth facies (Figures 4 and 15). The outermost of these ridges reaches heights of >80 m and can be traced for >300 km, actually crossing and extending beyond the ridged facies along the northern fan-shaped deposit boundary onto the surrounding Tharsis plains. Most of these secondary ridges are not concentric to the margins of the fan-shaped deposit and cannot be classified as members of the ridged facies due to their superposition and alternate orientations. Instead, they appear to be concentric to the present margins of the smooth facies, and are most pronounced to the north of the smooth facies (Figure 15). This apparent relationship with the smooth facies suggests that the ridges may have formed during retreat of a larger smooth facies deposit. However, these ridges are not as numerous, continuous or closely spaced as members of the ridged facies, which may result from different depositional conditions or timescales for formation.

[41] The smooth facies at Pavonis Mons provides further evidence for nonpolar, surficial ice deposits on Mars. Analysis of recent data from the High Resolution Stereo Camera (HRSC) on board Mars Express has revealed many features in the equatorial regions that appear to be ice-rich [*Neukum et al.*, 2004]. For example, collections of lobate features originating on the western Olympus Mons basal scarp have been interpreted as debris-covered glaciers [*Milkovich and Head*, 2003; *Neukum et al.*, 2004]. On the basis of crater counts for HRSC image data, these features appear to be 130–280 Ma with some subunits yielding ages of 20–60 Ma [*Neukum et al.*, 2004]. In addition, several other features observed in HRSC data have been interpreted as debris-covered glaciers elsewhere on the planet at low

latitudes [*Neukum et al.*, 2004; *Head et al.*, 2005]. Many of these glacial deposits appear to contain preserved subsurface volatiles due to a significant debris lag deposit [*Head et al.*, 2005]. This lag (or sublimation till) apparently retards sublimation sufficiently to allow significant volumes of water ice to survive near the equator, despite thermodynamic disequilibrium nearer to the surface.

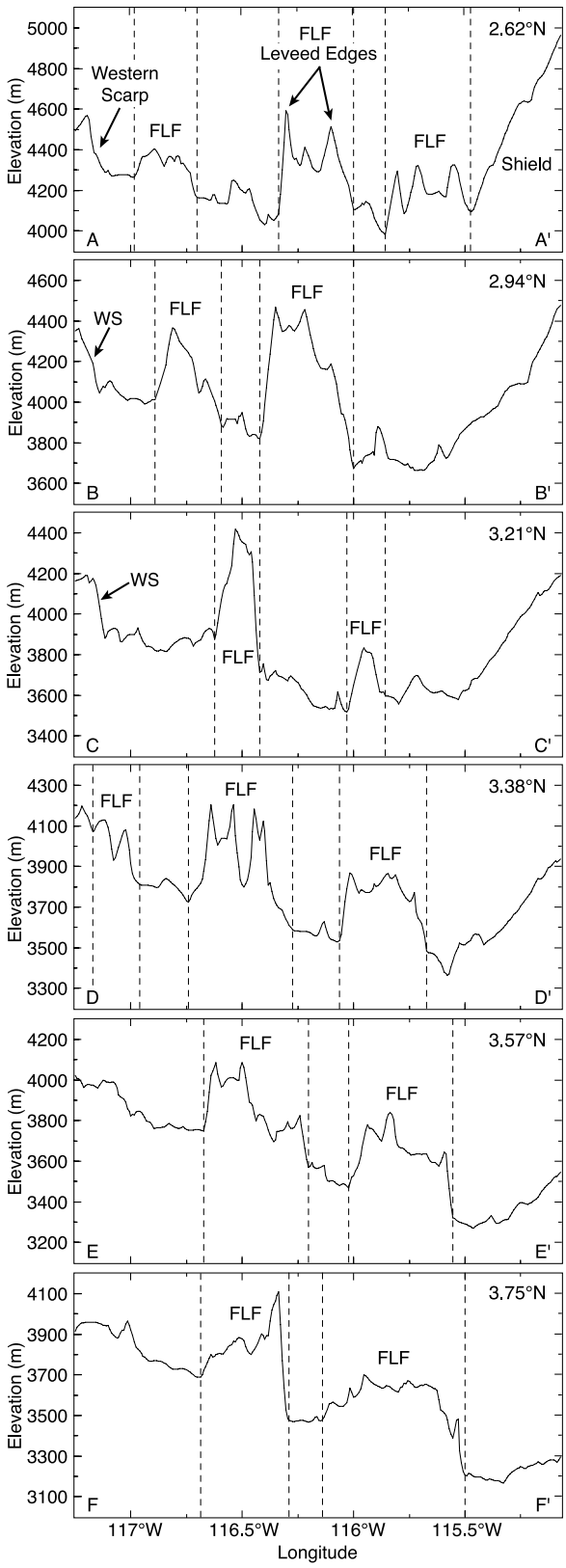

3.4. Lobate Flow-Like Features

[42] Two areas of unique lobate flow-like features exist in the western and north-central regions of the fan-shaped deposit (Figures 4 and 13). These features appear to be lava flows on the basis of their general shape; however, they are morphologically distinct from subaerial lava flows at higher elevations on the flanks of Pavonis and the digitate Tharsis Plains flows beyond the fan-shaped deposits to the west. They are characterized by elevated plateaus with leveed edges and steep walls, some with a relief of >500–600 m (Figures 13 and 18). Images of these lobate features reveal that they are superposed in places by the knobby facies, which continues uninterrupted onto the surrounding terrain (Figure 13). On the basis of this observation, these features have been previously interpreted as members of the knobby facies [*Scott et al.*, 1998]; however, MOLA topography data reveal that they are clearly elevated plateaus beneath the relatively thin veneer of the knobby facies (Figure 13).

[43] On the basis of Viking data, *Scott et al.* [1998] identified the edges of the lobate features as elongate, sinuous ridges and suggested that they might be eskers formed by deposition of sedimentary material beneath or within a wasting ice sheet. As mentioned before, MOLA topography data have revealed that these features are not simply ridges, but are continuous, elevated edges on plateaus. Due to their (1) lobate nature, (2) elevated topography, and (3) apparent relationship with fissures on the western flanks [*Zimbelman and Edgett*, 1992; *Scott et al.*, 1998], we agree with *Zimbelman and Edgett* [1992] and the alternative hypothesis of *Scott et al.* [1998] that these features are lava flows. *Zimbelman and Edgett* [1992] suggest that these features may be basaltic pyroclastic flows originating from troughs on the lower western and northeastern flanks of Pavonis Mons or from mostly buried troughs in the fan-shaped deposit. They propose that pyroclastic activity could have been triggered by the release of a lithostatic load resulting from a large landslide event that would have formed the fan-shaped deposit. However, the proposition that these flows postdate the other units within the fan-shaped deposit is inconsistent with the observations that show superposition of the knobby facies over both the western and northeastern lobate features. In addition, it is

Figure 18. MOLA profiles extracted from 128 pixel/degree gridded data across western lobate flow-like features. Refer to Figures 6 and 13 for context and profile locations. Dashed lines delineate the margins of individual flow-like features. Note the relief of the western scarp in profiles A, B, and C. The flow-like features have unique leveed edges that are apparent in nearly all profiles. Profile D-D′ provides an excellent example of several flow-like features with leveed edges that attain heights of >150 m above the center of the flow-like features. The unusually high relief of the flow-like features is also apparent in the profiles, specifically in B-B′ and C-C′ where flows achieve heights of >600 m above the surrounding terrain. Vertical exaggeration is 60X.

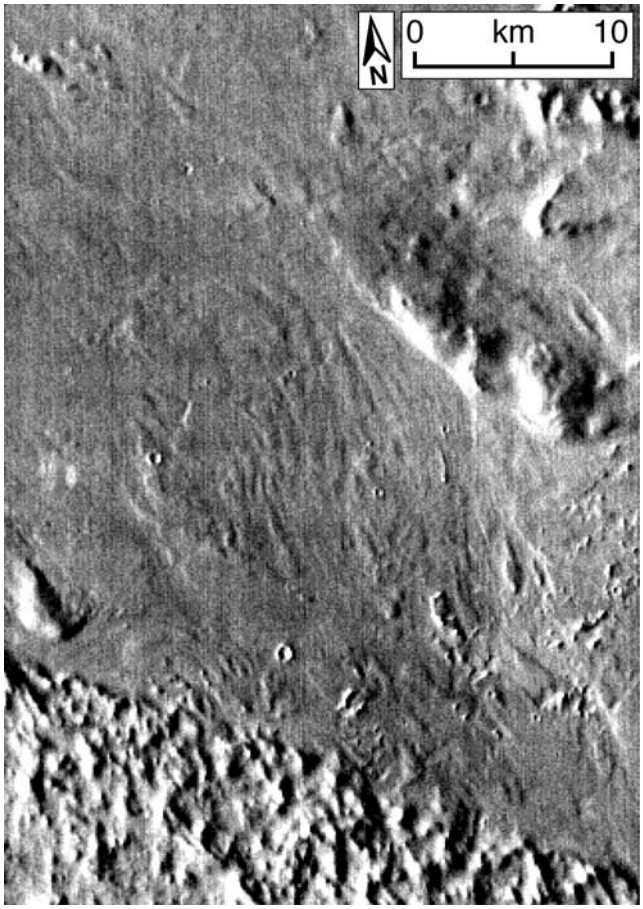

Figure 19. THEMIS daytime IR image showing candidate fluvial features northeast of the Pavonis fan-shaped deposit (Image I02438002). These features may have been produced by meltwater outflow from localized wet-based activity as a result of subglacial eruptions beneath a glacier at Pavonis Mons.

unlikely that the unusually steep scarps and observed relief of the lobate flow-like features could be produced by pyroclastic flows.

[44] *Zimbelman and Edgett* [1992] proposed an alternate hypothesis to a pyroclastic origin, suggesting that these features comprise a series of highly viscous flows emanating from the troughs on the western and northeastern flanks prior to the development of the fan-shaped deposit. This explanation is plausible within our glacial model, assuming that such flows would have sufficient time to cool and could later be covered by a glacier with a thickness greater than 600 m. As the glacier underwent retreat, its debris load would be deposited directly onto the underlying terrain, regardless of topography. This model could potentially explain both the unusual relief of these features and the superposition of the knobby facies. However, we have not observed any lava flows within Tharsis or other volcanic provinces on Mars that bear any resemblance to these unusual lobate features. They are only observed within the fan-shaped deposits of Pavonis Mons and potentially Ascraeus Mons, indicating that a relationship with the fan-shaped deposits may be present.

[45] An alternative explanation for these features involves subglacial eruptions beneath a relatively thick cold-based glacier [e.g., *Wilson and Head*, 2002]. We have attempted to identify sources for these lobate features, using previous maps as a guide [*Zimbelman and Edgett*, 1992; *Scott et al.*, 1998] and have mapped out our interpretation of flow direction using topography and image data (Figure 13). The subglacial model is consistent with superposition relationships and may provide an explanation for the unusual morphology, aspect ratio, and relief of the flows. The leveed edges and steep scarps may represent chilling at the margins of the lava flows during emplacement, forcing the flows to propagate upward through the overlying ice.

[46] However, this model also has several shortcomings. For example, subglacial flows of this volume would be expected to generate a significant amount of heat and meltwater. Ponding of this meltwater could eventually lead to release, which would be expected to leave behind characteristic morphological features such as subglacial drainage networks, broad channels (similar to those carved by terrestrial jökulhlaups), or outwash plains depending on the volume of water released and discharge rate. We have not observed any characteristic features indicative of large releases of meltwater reservoirs in regions immediately surrounding the flows. However, it is interesting to note that the distribution of the knobby facies around these flow-like features and other potential subglacial volcanic features is highly unusual (see section 3.2, Figure 13). This observation may be related to localized meltwater activity selectively stripping sections of the knobby facies to produce the patches devoid of the knobby facies. In addition, at least one channel is present in proximity to the western flow-like features that may be related to meltwater drainage (Figure 10). Finally, there appear to be a collection of candidate fluvial features off the northeastern boundary of the Pavonis fan-shaped deposit (Figure 19). If these features are fluvial in nature, they may have been carved by meltwater outflow from a glacier at Pavonis Mons. The source of these channels could have been meltwater generated by the northern lobate flow-like features intruding into overlying ice. However, it is important to note that these northern lobate features are at least 100 km from the purported fluvial channels and we do not see any similar meltwater features *within* the fan-shaped deposit.

3.5. Linear Radial Ridges

[47] In addition to the lobate flow-like features, we have identified six linear or curvilinear ridges in the central regions of the Pavonis fan-shaped deposits that are independent of the ridged facies and secondary ridges (Figures 4 and 13). Recall that the ridged facies consists of parallel, concentric ridges that are most pronounced around the distal margins of the Pavonis deposit and in the central, proximal regions of the deposit (Figures 4 and 9). The secondary ridges discussed earlier superpose the ridged facies and are concentric to the present margins of the smooth facies (Figure 15).

[48] These additional linear ridges are radial to the base of the shield and have dimensions of approximately 100–200 m high, 1 km wide, and 30–60 km long (Figure 20). All ridges are roughly linear except for one curvilinear ridge that continues beneath the main smooth facies deposit

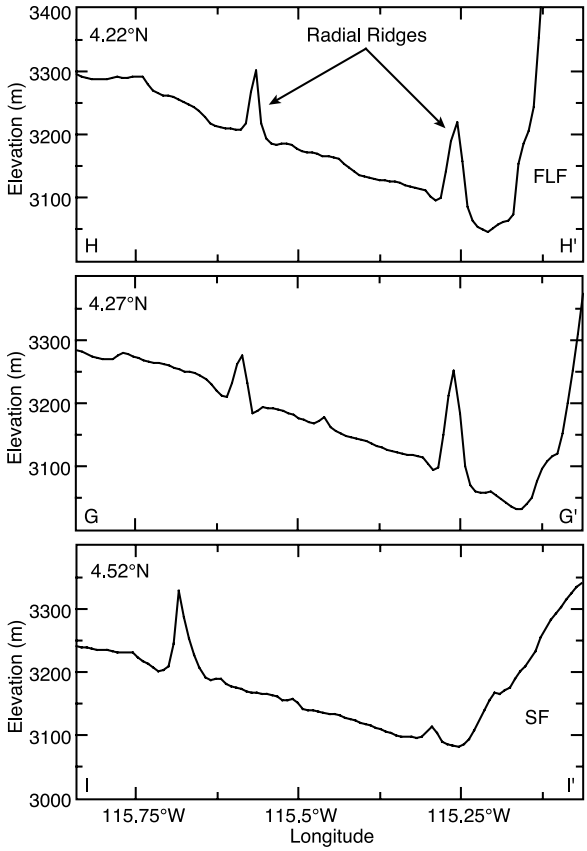

Figure 20. MOLA profiles of the two largest radial ridges at Pavonis extracted from 128 pixel/degree gridded data. Despite the limitations in resolution of the gridded MOLA data, the radial ridges display a relief of over 150 m above the surrounding terrain. Vertical exaggeration is 57X.

(Figures 4, 13, and 17). Another radial ridge appears to enlarge into an 8 km wide pancake-like feature with a small depression at its center (Figure 13). Two other ridges originating on the northwestern flanks of Pavonis Mons appear en echelon in plan view while others display forking or splitting in places (Figures 13, 17, and 21b).

[49] These ridges have previously been interpreted as levees at the margins of a broad flow channel [*Hodges and Moore*, 1994] and as eskers [*Scott et al.*, 1998]. On the basis of their (1) radial orientation with respect to the shield, (2) peaked cross section in MOLA profiles, and (3) forked or en echelon nature, we interpret these features as radial dikes, which may have erupted in a subglacial environment [e.g., *Wilson and Head*, 2002]. Analysis of high-resolution MOC images reveals that some of the radial ridges appear to have split peaks, plateaus and even elongated collapse pits along the central ridge axis (Figure 21). These features suggest that the ridges interpreted as dikes were emplaced beneath a relatively thick glacier and may have encountered variable stresses within the ice where local pressure conditions allowed for the formation of such structures. The unusual pancake-like feature associated with one of the radial ridges (Figure 13) may also represent a sill that formed subglacially during dike emplacement.

[50] Several questions regarding the origin of these radial ridges and lobate flow-like features remain unanswered. The most pressing of these questions include (1) when did these features form in relation to other units within the Pavonis fan-shaped deposit, (2) why do we not see similar flows or dikes elsewhere on Mars, (3) why do the flows have such steep scarps and unusual leveed edges, and (4) if these features formed subglacially, why do we not see more evidence of erosional features suggesting the presence of meltwater in proximity to the flows? Further in-depth analysis of new data of the Pavonis fan-shaped deposit and of terrestrial subglacial eruptions will be required before a comprehensive hypothesis explaining these features can be formulated.

3.6. Arcuate Scarps

[51] In addition to the volcanic features described above, three arcuate scarps are observed within the Pavonis Mons fan-shaped deposit (Figure 4). The most prominent scarp is located where the Pavonis deposit is bounded to the east by lava flows that comprise the Tharsis Plains (Figure 15). MOLA profiles across this scarp reveal that the fan-shaped deposits are up to 200 m lower than the surrounding lava plains (Figure 22). It appears that lava flows from the east were prevented from flowing toward lower elevations for >80 km along the scarp and instead continue to the north-northwest before resuming the path expected on the basis of the local topography (Figure 15). This is precisely the behavior that we would expect assuming that a large glacier with a relief of >200 m existed at the time of lava flow emplacement. Analysis of regional-scale image mosaics and topography data shows that a lip of the knobby facies is observed 5–10 km eastward of the scarp on the elevated lava flows (Figures 15 and 22). This lip appears to be the result of glacial advance following the formation of the scarp, with subsequent retreat and deposition of debris during the emplacement of the knobby facies. One possible model to explain the scarp and associated lip involves four essential steps (Figure 23). First, we assume that a large glacier existed with its outer margins at the location of the scarp (Figure 23a). Next, a series of late-stage flows from Pavonis or Ascraeus Mons traveled downslope and were deflected toward the north-northwest by the glacier at Pavonis (Figure 23b). Additional advance of the ice extended the coverage of the glacier by another 5–10 km onto the cooled lava flows (Figure 23c). Finally, due to changing climatic conditions the ice began to sublimate and retreat, depositing its debris load to form the knobby facies of the Pavonis fan-shaped deposit (Figure 23d).

[52] Two additional scarps are present within the Pavonis deposit, although they are not as well defined as the prominent eastern scarp. The second arcuate scarp is observed approximately 20–30 km from the northeastern margin of the fan-shaped deposit (Figure 4) and has a relief of nearly 100 m in places (Figures 15 and 24). This inner eastern scarp is approximately concentric to the margins of the Pavonis fan-shaped deposit and can be traced for >120 km (Figures 4 and 15). The ridged facies, knobby facies, and younger secondary ridges are all superposed on this scarp, indicating that it was formed early in the history of the Pavonis fan-shaped deposit, prior to their deposition. MOLA profiles indicate that this scarp may actually be the inner edge of an elevated band, concentric to the margins of the deposit along the outer 20–30 km of the northwestern

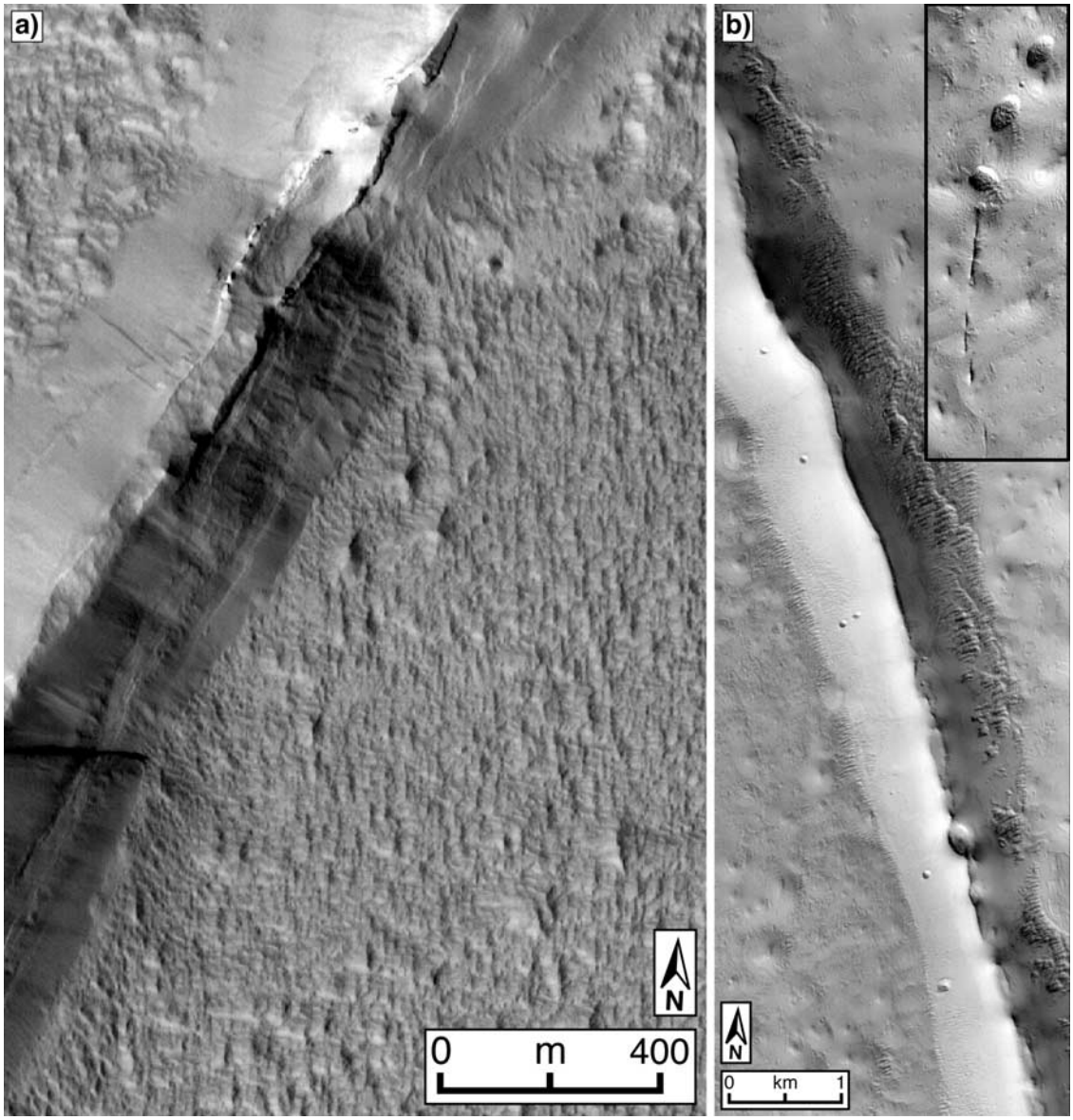

Figure 21. MOC narrow-angle images of radial ridges: (a) section of curvilinear radial ridge showing split peak and outcrop along central ridge axis (Image M0805337). The radial ridges are interpreted as dikes possibly erupted in a subglacial environment. (b) Another radial ridge showing splitting and collapse pits along the central ridge axis (Image E1300839). The inset image is located approximately 15 km north-northwest of the radial ridge. The features in the inset appear to represent an en echelon offshoot of the main dike that transitions into elongated collapse pits, suggesting an interaction with volatile-rich material during emplacement.

regions (Figures 15 and 24). This band is typically ~50–70 m above the surrounding terrain with relatively steep scarps defining its inner and outer boundaries. The highly concentric distribution and elevated relief of this band indicate that it may not be the result of volcanic flows, but could represent material associated with the initial phases of glaciation at Pavonis.

[53] The third arcuate scarp of the Pavonis fan-shaped deposit is observed approximately 30–50 km to the east of the western margin of the deposit (Figure 4). This western scarp is covered by the knobby facies and lies to the west of the western lobate features (Figures 13 and 18). MOLA topography reveals that it is approximately 120–130 km long, and has a relief of >350 m in places (Figures 13 and 18). Assuming this scarp was formed by lava flows banking up against an early glacier suggests that the earliest ice sheet at Pavonis had a relief of >350 m. Superposition relationships suggest that the formation of this scarp occurred early in the evolution of the fan-shaped deposit, possibly during the initial phases of glaciation at Pavonis.

3.7. Terrestrial Glacial Analogs

[54] Glaciologists generally classify terrestrial glaciers as either wet-based or cold-based, depending on their basal thermal conditions. Within a wet-based or temperate glacier, the pressure of overlying ice is sufficient to induce pressure

melting. These glaciers advance both through internal deformation and sliding along the base via a layer of meltwater, often producing distinctive erosional and depositional features such as terminal moraines, eskers, drumlins, flutes, and bedrock striations. On the Earth, these glaciers are typically found at low to midlatitudes.

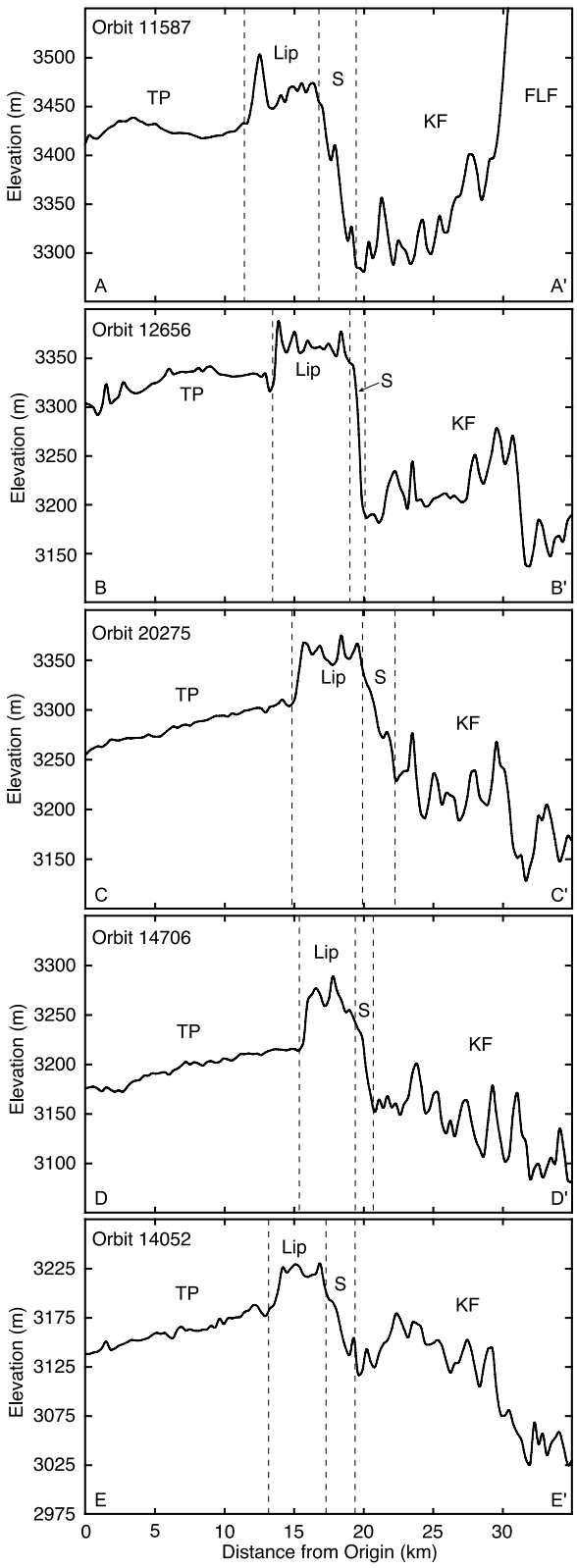

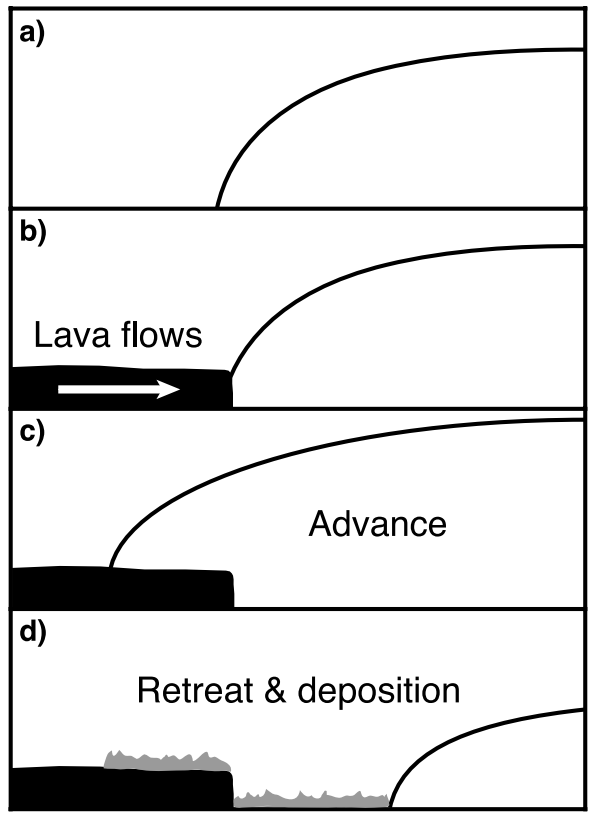

Figure 23. Formative mechanism for the eastern scarp involving four major steps: (a) ice sheet margins extend to present location of scarp, (b) lava flows from the east bank up against ice sheet and cool, (c) ice sheet advances an additional 5–10 km onto the cooled and solidified lava flows, and (d) glacial retreat and deposition of knobby facies over newly formed scarp. This model effectively explains the apparent northward deflection of lava flows comprising the Tharsis Plains, the relief of the eastern scarp, and the presence of a 5–10 km lip of the knobby facies on the flows to the east of the scarp.

[55] The second type of terrestrial glacier is known as a cold-based or polar glacier. Basal temperatures in cold-based glaciers are below the pressure melting point; as a result, these glaciers remain frozen to their beds and do not slide along the bedrock interface. Instead, advance only

Figure 22. MOLA profiles taken from individual orbits across the eastern scarp. Refer to Figure 6 for profile context and Figure 15 for MOLA gridded data of the eastern scarp. Dashed lines separate the sections of the profiles. The Tharsis Plains east of the Pavonis fan-shaped deposit are labeled "TP". The lip of the knobby facies (labeled as "Lip") is present on the Tharsis Plains beyond the scarp and is typically 5–10 km wide with a relief of <50 m. The actual scarp is labeled "S" and is best represented in profile B-B′ where its relief exceeds 150 m. Inward of the scarp is the knobby facies (KF) which displays a relief of ~10–70 m and is superposed on underlying topography. Vertical exaggeration is 53X.

occurs through internal deformation allowing for relatively slow ice and debris transport from accumulation zones to ablation zones. Little or no ice movement occurs at the base while the highest ice velocities are found near the surface of the glacier. Terrestrial field observations of cold-based glaciers show that they passively deposit their debris load on the underlying topography in the form of characteristic features such as drop moraines or sublimation tills with little or no bed modification [*Rains and Shaw*, 1981; *Benn and Evans*, 1998; *Head and Marchant*, 2003]. They are typically found in arid, polar regions such as the Dry Valleys of Antarctica where extremely low temperatures and precipitation rates prevent conditions favoring wet-based glacial activity.

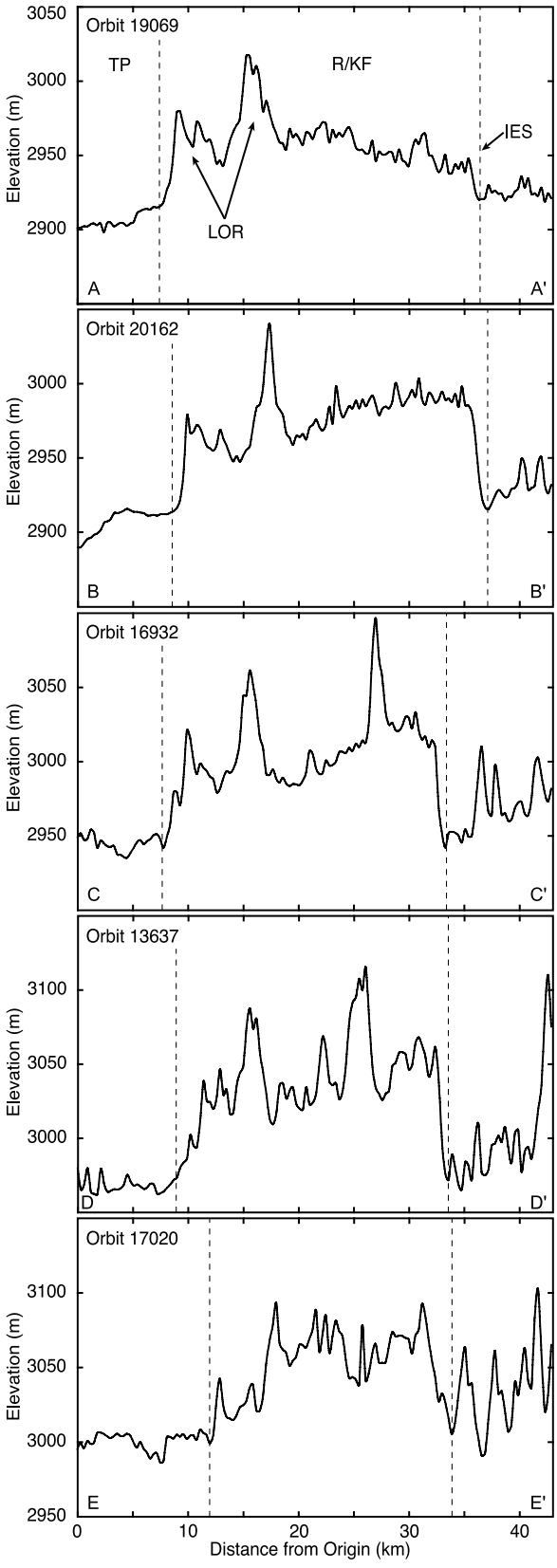

[56] Under current Martian climate conditions, any glacial activity is more likely to be cold-based (similar to terrestrial polar glaciers) as opposed to wet-based [*Head and Marchant*, 2003]. We believe that the fan-shaped deposit at Pavonis Mons provides additional evidence for the former presence of cold-based glacier(s) on the northwestern flanks in recent Martian history. The three characteristic facies of the Tharsis Montes fan-shaped deposits are all present within the deposit at Pavonis Mons, and all can be interpreted as features commonly associated with terrestrial cold-based glaciers. The ridged facies bears a striking similarity to terrestrial drop moraines associated with recession, stagnation and deposition by cold-based glaciers such as those in the Antarctic Dry Valleys (Figure 12a) [*Head and Marchant*, 2003]. The knobby facies appears to represent a sublimation till, produced during the down-wasting of debris-rich ice (Figure 12b) [*Head and Marchant*, 2003]. Finally, the smooth facies at Pavonis Mons resembles debris-covered ice that may have experienced localized rock-glacier-like flow (Figure 12c). The superposition relationships and morphology of the three main facies suggest that at least three major episodes of debris deposition have occurred, likely under disparate or evolving climatic conditions. In addition, very few features suggesting the presence of meltwater have been observed *within* the Pavonis fan-shaped deposit. The only evidence for large-scale fluvial activity that may be associated with the Pavonis deposit and/or related volcanism is observed off the northeastern margin; however, a direct relationship with the Pavonis fan-shaped deposit cannot be inferred on the basis of available data. Fluvial activity is rarely associated with cold-based glaciers, so the presence of characteristic glacial landforms such as moraines with an absence of meltwater features or bed modification suggests that glaciation was primarily cold-based.

Figure 24. MOLA orbit profiles of the concentric band of material in the northeastern regions of the Pavonis fan-shaped deposit and inner eastern scarp. Refer to Figure 6 for profile context and Figure 15 for gridded MOLA data of the concentric band. In each profile the extent of the band is outlined by dashed lines. The line on the left side delineates the boundary between the Tharsis Plains (TP) to the northeast and the Pavonis fan-shaped deposit. Within this boundary, sections of the large outer ridges can be identified as in profiles A, B, and C. The dashed line to the right identifies the location of the inner eastern scarp, which can attain a relief of over 70 m in places. The concentric band is typically 20–30 km wide and is superposed by the ridged facies and the knobby facies, suggesting it formed early in the history of the Pavonis fan-shaped deposit. Vertical exaggeration is 133X.

[57] It should be noted that the two classes for glaciers are simply end-member models for ideal ice behavior. In reality, many terrestrial glaciers are polythermal with a spatially variant temperature regime due to differences in bed topography, flow rates, and ice thickness [*Rains and Shaw*, 1981; *Benn and Evans*, 1998]. For example, in the thinner, more distal regions of a polythermal glacier, thermal conditions could be cold-based, while in the thicker, proximal areas (specifically accumulation zones), glacial behavior could be wet-based.

[58] No evidence for wet-based glacial features within the fan-shaped deposit was documented at Arsia Mons [*Head and Marchant*, 2003]. However, at Pavonis we do see elongated knobs which in the past have been interpreted as drumlins (Figure 10) [*Scott et al.*, 1998] and possible channels carved by meltwater outflow (Figure 19). The presence of such features could indicate that periods of isolated wet-based glacial activity may have occurred at Pavonis. Observations of terrestrial wet-based glaciers indicate that they typically scour their bed, destroying previous depositional features in the process. On the contrary, cold-based glaciers (or the cold-based portions of polythermal glaciers) passively advance over the underlying bed through internal deformation with insignificant modification of underlying features [*Head and Marchant*, 2003]. Thus, if wet-based glacial activity ever occurred at Pavonis, we would not expect to see well-preserved, underlying depositional features such as drop moraines. The fact that we do see these features indicates that any wet-based glacial activity was locally isolated or could have taken place before the deposition of the three characteristic facies. However, the candidate drumlin fields appear to be members of the knobby facies and are superposed on the underlying ridged facies, suggesting that they could not have been formed through subglacial bed modification without destroying the ridges. Clearly, there are still many questions that remain unanswered regarding the role, if any, that wet-based glacial activity has played in the formation of the Pavonis deposit and the answers to these questions will only come with analysis of new data and three-dimensional ice sheet modeling efforts.

3.8. History of Pavonis Fan-Shaped Deposit

[59] The Pavonis fan-shaped deposit has undoubtedly had a complex history that appears to involve glaciation, volcanism, and later modification by erosion. We have documented evidence suggesting that several phases of glaciation and deposition occurred during the evolution of the deposit. Here, we outline our interpretation of its history, from the earliest stages of glaciation to the present:

[60] Figure 25a: Final stages of Pavonis Mons shield construction and late-stage flank vent eruptions during the Late Amazonian [*Scott et al.*, 1998].

[61] Figure 25b: Glacier develops on the west-northwestern flanks and begins to advance onto the surrounding plains.

[62] Figure 25c: When ice extends approximately 80 km from the base of the shield, a series of lava flows from the south bank up against the glacier, cool and form the western arcuate scarp.

[63] Figure 25d: Glacier advance continues to north-northwest for another 100–150 km. A glacial maximum is reached at the observed outer boundary of the fan-shaped deposit.

[64] Figure 25e: An extended period of dynamic equilibrium ensues; large outer ridges are deposited.

[65] Figure 25f: A period of regular and systematic retreat and stability ensues, depositing drop moraines to within 70 km of the shield.

[66] Figure 25g: Second major phase of advance commences, eventually covering a large portion of the previous deposits. Debris cover is inhomogeneous, with dense distribution to the northeast and west. Glacial surface topography may be variable.

[67] Figure 25h: Formation of lobate features and radial ridges (?).

[68] Figure 25i: Subaerial lava flows from the east bank up against the glacier and is deflected to the north, forming the well-defined eastern scarp.

[69] Figure 25j: Additional advance of the glacier for at least 5–10 km beyond this scarp.

[70] Figure 25k: Relatively rapid sublimation of ice to deposit the knobby facies.

[71] Figure 25l: Third major phase of advance begins. This phase reaches its maximum as defined by the outermost of the secondary ridges.

[72] Figure 25m: Sporadic retreat of this glacier occurs, leaving secondary ridges during longer periods of stagnation and down-wasting or increased debris accumulation (possibly from intermittent volcanic eruptions). The current manifestation of this phase is the smooth facies, which may be experiencing rock-glacier-like flow.

[73] Figure 25n: Eolian modification and erosion.

4. Ice Sheet Models

[74] Terrestrial ice sheet models can be employed to further test a cold-based glacial hypothesis for the Tharsis Montes fan-shaped deposits. Reconstruction of these glaciers provides estimates for ice thicknesses and volumes, which will help delineate the thermal character of the ice (cold-based versus wet-based) and any lateral variation of this thermal character within the glaciers. More importantly, these estimates can be compared to current polar-cap volumes on Mars, providing information regarding the amount of material removed from volatile reservoirs and the global distribution of volatiles during the time when the Tharsis Montes glaciers were present.

[75] Observations of the shape, distribution, and elevations of the Tharsis Montes fan-shaped deposits can provide important constraints for ice sheet reconstruction. In plan view (Figure 1), all three deposits are lobate in nature, extending onto the relatively flat plains to the west-northwest of each shield with thinning ''horns'' that taper to a point at higher elevations on the shield flanks (Figure 1). However, they differ greatly in size and orientation with respect to the shield (Table 1).

[76] Identifying and characterizing the accumulation zones for these glaciers is critical to understanding their nature. The shape and orientation of all three deposits constrain the accumulation zones to the west-northwest flanks of each shield. As ice thicknesses in the accumulation zones began to increase, gravity-driven flow would occur down the flanks with significant lateral spreading upon

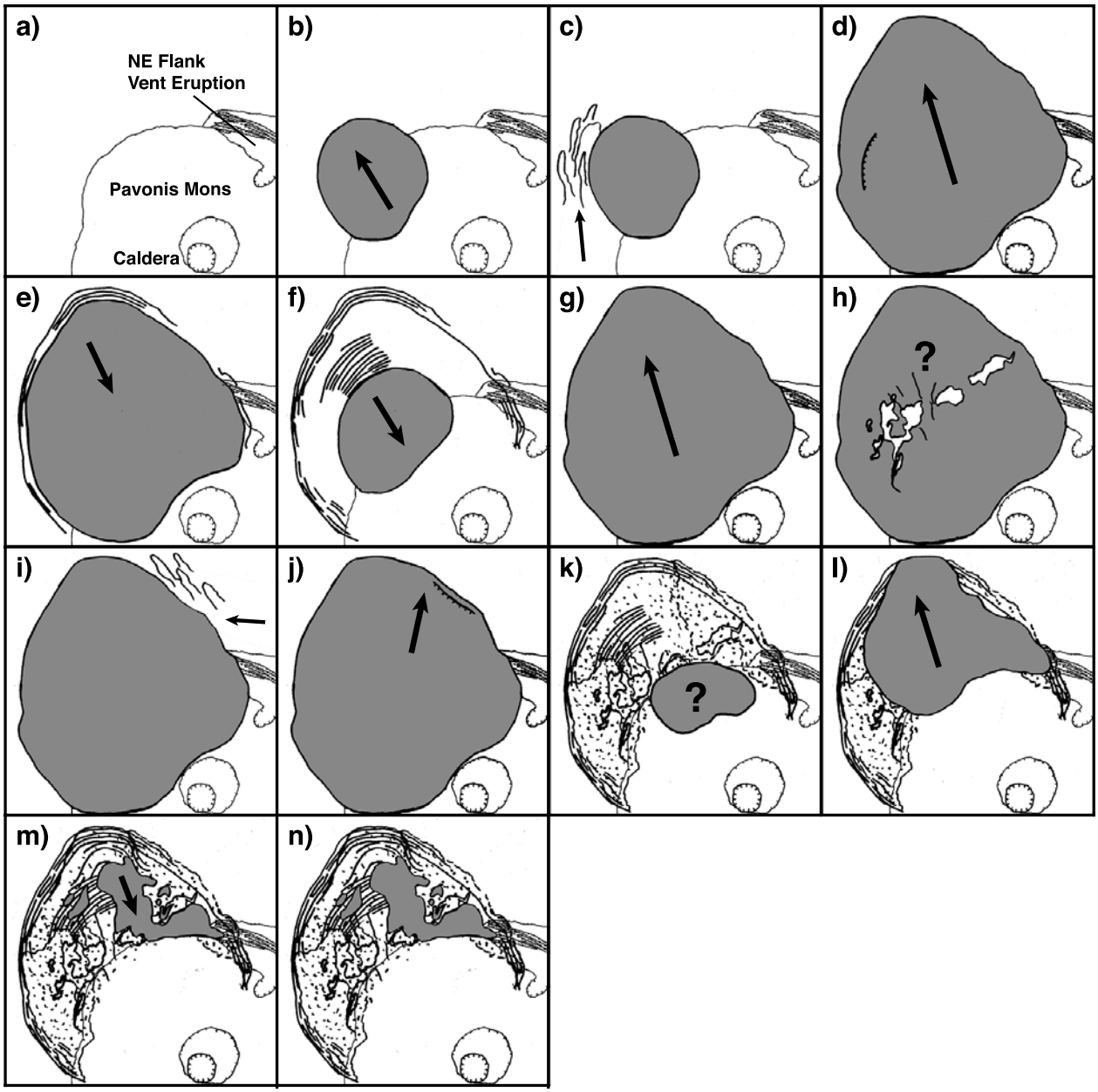

Figure 25. History of the Pavonis fan-shaped deposit. Arrows indicate the significant event at each stage, and ice is always shaded. (a) During the Mid to Late Amazonian, major construction of the Pavonis Mons shield ceases and late stage flank vent eruptions occur, (b) a glacier develops on the west-northwestern flanks and begins to advance onto the surrounding plains toward the west-northwest, (c) when ice extends approximately 80 km from the base of the shield, a series of lava flows from the south bank up against the glacier, cool, and form the western arcuate scarp, (d) glacial advance continues to the north-northwest for another 100–150 km and a glacial maximum is reached at the observed outer boundary of the fan-shaped deposit, (e) retreat slowly begins and the large outer ridge is deposited, followed by additional outer ridges, (f) a period of regular cyclical retreat ensues, depositing drop moraines to within 70 km of the shield, (g) second major phase of advance commences, eventually covering a large portion of the previous deposits, (h) emplacement of lobate flow-like features and radial ridges (?), (i) subaerial lava flows from the east bank up against the glacier and is deflected to the north, forming the eastern scarp, (j) additional advance of the glacier for at least 5–10 km beyond this scarp, (k) relatively rapid sublimation and down-wasting of ice to deposit the knobby facies; some remnant ice may persist in the thicker central regions of the glacier during the deposition of the knobby facies, (l) third major phase of advance begins and reaches maximum at the outermost of secondary ridges, (m) sporadic retreat of this glacier occurs, leaving secondary ridges during longer periods of stagnation or increased debris accumulation (possibly from intermittent volcanic eruptions), and (n) current manifestation of this phase is the smooth facies.

encountering the break in slope at the base of each shield. In addition, we know that the accumulation zone at each shield would have been higher than the maximum elevations of the deposits (Table 1).

[77] The shape and elevations of the "horns" at each deposit provide further constraints for the size and location of the accumulation zones. At Arsia Mons, the "horns" on both the southwestern and northeastern flanks have been partially obscured by subsequent lava flows (Figure 1). For this reason, the values given for maximum fan-shaped deposit elevation at Arsia Mons should be considered the minimum values for the elevation of the accumulation zone. The actual deposit may have once been present at higher elevations, tapering to a point similar to the "horns" of the deposit at Pavonis Mons.

4.1. Regional Topography Considerations

[78] Observations of the size and orientation of the fan-shaped deposits suggest that the local topography had a significant effect on both the direction of ice flow and final distribution of the ice sheets at each shield. When considering the Tharsis Montes region as a whole, a general northwesterly slope is observed (Figure 1) [*Zimbelman and Edgett*, 1992]. However, MOLA data reveal that the local topography and slopes northwest of each shield are distinctive (Figures 1 and 26).

[79] The elevation of the caldera rim at Arsia Mons is approximately 17.0 km with an average slope of ~6° on the west-northwestern flanks. At an elevation of ~5.5–6.0 km, a break in slope is observed upon reaching the surrounding plains which slope gently (~0.5°) to the west-northwest. As would be expected for glacial behavior, the trend of the Arsia Mons fan-shaped deposit closely follows the average slope direction of the local topography northwest of the shield (Figure 26).

[80] The caldera rim at Pavonis has an elevation of approximately 14.0 km with an average slope of ~4° on the northwestern flanks. North of the shield, slopes are gentle (<0.3°) to the northwest (Figure 26). However, the broad topographic rise to the west of Pavonis Mons (Figure 1; see section 3), produces easterly slopes of ~1–2° (Figure 26). This rise would be expected to deflect glacial advance to the north and may explain the more northerly trend (N27°W) of the Pavonis fan-shaped deposit.

[81] The caldera rim of Ascraeus Mons has the highest elevation of the three Tharsis Montes at around 18.0 km, coupled with the steepest slopes on the west-northwestern flanks of ~8°. Although the magnitudes of the local slopes to the west-northwest of Ascraeus are small (~0.1–0.4°), the direction of these slopes forms a depression directed inward toward the shield that contains the Ascraeus Mons fan-shaped deposit (Figure 26). This depression would have influenced advance of the Ascraeus glacier and may help explain the smaller size of the Ascraeus deposit.

[82] Due to the young age of the deposits, we can assume that the topography northwest of the Tharsis Montes has not changed significantly since the time when these glaciers were present. In addition, the large crustal thicknesses beneath the Tharsis Montes (>90 km [*Zuber et al.*, 2000]) suggest that a few kilometers of glacial ice would have little impact on the isostatic equilibrium of the region. In summary, the overall orientation, shape, and distribution of the fan-shaped deposits are consistent with the local topography west-northwest of each shield, and the deposits are located precisely where we would expect to see glacial advance assuming accumulation was occurring on the west-northwestern flanks of the Tharsis Montes.

4.2. Steady-State Profile Model

[83] The basic inputs of all ice sheet models include gravity, ice density and ice yield stress τ_0 (0.5–1.5 bar [*Nye*, 1952]). The yield stress in this context is the pressure at which a column of ice will flow laterally, reducing total thickness. For simplification, many models assume that ice is a perfectly plastic substance with basal shear stress equal to the yield stress along the entire ice sheet profile. Reconstructions of present-day terrestrial ice sheets using this technique show that this is a valid assumption for most cases [e.g., *Nye*, 1952; *Denton and Hughes*, 1981; *Reeh*, 1982]. The choice of a realistic yield stress is critical, considering that nearly every ice sheet model involves a factor of $(\tau_0/\rho g)$ for thickness estimates. Higher values of τ_0 correspond to "harder" ice, resulting in greater ice thicknesses and reduced lateral extent while lower values of τ_0 correspond to "softer" ice, resulting in reduced ice thicknesses and greater lateral extent. Values for τ_0 have been empirically derived for present-day cold-based ice sheets with an average of around 1.0 bar [*Denton and Hughes*, 1981].

[84] A reconstructed ice sheet profile was generated for each of the three Tharsis Montes glaciers. Base MOLA topography profiles (~0.5 km spacing between points) were extracted along a single flow line connecting the caldera and the most distal moraine of the fan-shaped deposit at each of the Tharsis Montes (Figure 1). These flow lines coincide with the maximum elongation of the deposit and thus provide estimates for maximum ice thicknesses when used as model inputs. Along each flow line, an iterative steady state profile for perfectly plastic ice with a yield stress of 1.0 bar was constructed. The first step from the outer margin of the deposit was defined as a simple parabolic snout [e.g., *Nye*, 1952; *Denton and Hughes*, 1981; *Rains and Shaw*, 1981] and each step thereafter was determined by the following equation for the elevation of the ice sheet surface (h_{i+1}) [*Denton and Hughes*, 1981]:

$$h_{i+1} = h_i + \left(\frac{\tau}{\rho g}\right)\left(\frac{1}{h_i - r_i}\right)\Delta x, \quad (1)$$

where h_i is the elevation of the ice sheet surface at the previous step, τ is the yield stress (1.0 bar), ρ is the density of ice (0.917 g cm^{-3}), g is gravity (3.72 m s^{-2}), r_i is the elevation of the bed at the previous step and Δx is the step size (~0.5 km) (Figure 27).

4.3. Results

[85] As expected, all profiles generated using the above equation display a characteristic glacial profile with ice thicknesses increasing progressively from the snout of the glacier (Figure 28). The profiles also display an inverse relationship between ice thickness and slope (Figure 28). On the flanks of each shield (slopes ~3–8°), ice thicknesses are on the order of tens to a few hundred meters, while thicknesses approach 3.2, 3.1, and 2.1 km on the relatively

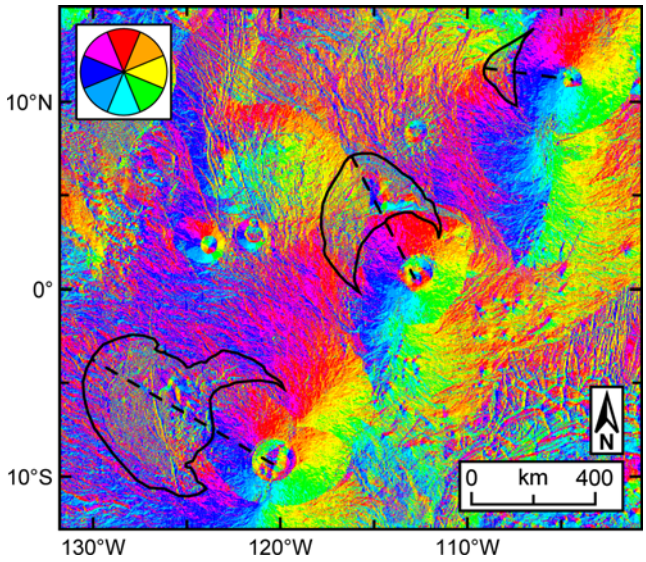

Figure 26. Aspect map of slopes in Tharsis generated using MOLA topography data. Slope direction is binned into 8 categories based on the color wheel in the upper left-hand corner. Terrain sloping to the north is colored red, terrain sloping to the northeast is colored orange, to the east, colored yellow, etc. The average slope surrounding the Arsia fan-shaped deposit is approximately 0.5° to the west-northwest, and the trend of the Arsia deposit (N62°W) generally follows the average slope direction of the underlying terrain. The broad topographic rise to the west of Pavonis Mons produces easterly slopes, while the terrain to the north of Pavonis Mons follows the regional northwesterly slopes. The Pavonis deposit displays the most northerly trend (N27°W) apparently due to the broad topographic rise west of Pavonis Mons, which is not a factor at Arsia or Ascraeus. Finally, the slopes to the west of Ascraeus Mons form a depression with shallow slopes directed inward toward the base of the shield. The Ascraeus fan-shaped deposit (N82°W trend) is located directly within this basin. The direction, shape, and overall distribution of the Tharsis Montes fan-shaped deposits are consistent with the local topography at each shield, suggesting that local slopes played an important role during glacial advance.

flat surrounding plains at Arsia, Pavonis, and Ascraeus, respectively (Figure 28). Simple thermal calculations reveal that basal temperatures beneath 2.1–3.2 km thick ice sheets on Mars are within the cold-based regime. It is important to note that these are estimates of maximum thicknesses for the glaciers that would have formed the fan-shaped deposits. Smaller ice thicknesses predicted along other flow lines are also consistent with a cold-based interpretation.

[86] Table 3 compares the average ice sheet thicknesses predicted using the MOLA topography along each flow line to thicknesses predicted by the same model on a flat, horizontal plane. This analysis confirms that even shallow slopes (e.g., <0.5° northwest of Arsia Mons) can have fairly significant effects (~31% difference) on thickness estimates for a fully equilibrated ice sheet on Mars. Thus the local topography at each of the Tharsis Montes would be expected to have a significant influence on glacier behavior and overall lateral distribution.

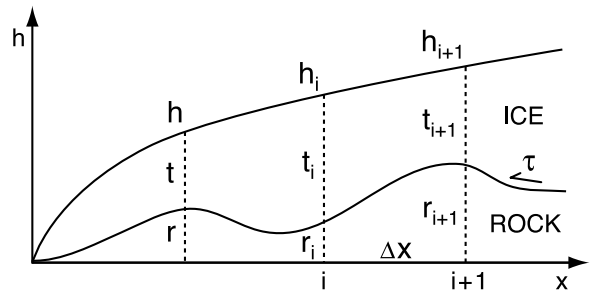

Figure 27. Profile model for ice sheet reconstruction using basal topography. Parameters shown include ice surface elevation (h), ice thickness (t), base elevation (r), horizontal step size (Δx), and yield stress of ice (τ) (modified from *Denton and Hughes* [1981]).

[87] More complex ice sheet models can account for non-steady-state conditions and require accumulation and ablation rates as inputs. Other variables that can influence ice behavior include atmospheric conditions, basal heat flux, and ice properties such as composition, internal temperature, and variable hardness. While some parameters are poorly constrained for Mars, these dynamic models can provide additional estimates for ice thickness with temporal variation [*Fastook et al.*, 2004]. The dynamic model of *Fastook et al.* [2004] was adapted for Mars and used to reconstruct the Arsia Mons glacier along a similar flow line as the flow line used for the reconstructions in Figure 28. These reconstructions yielded average equilibrated ice thickness estimates of approximately 2.0–2.1 km for Arsia Mons, values which are comparable to the estimates of the simple profile model of Table 3.

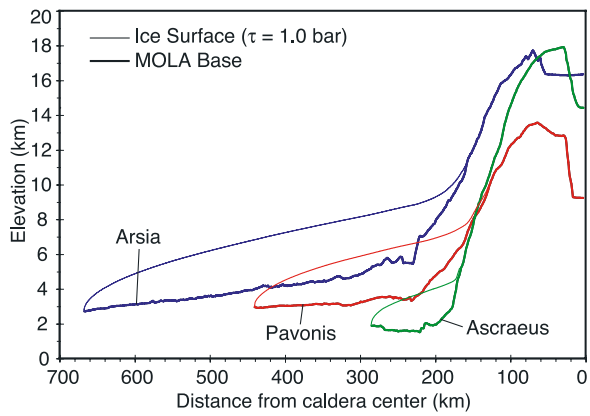

Figure 28. Reconstructed ice sheet profiles for the Tharsis Montes glaciers using the model of *Denton and Hughes* [1981] and a yield stress (τ) of 1.0 bar. Basal topography profiles were extracted from 128 pixel/degree gridded MOLA data from the caldera to the outermost ridge of the fan-shaped deposit at each of the Tharsis Montes. Refer to Figure 1 for the location of the MOLA profiles used in reconstructions and Table 3 for quantitative results. For each shield, MOLA topography is represented by a thick, solid line while a thinner line represents the reconstructed ice sheet surface. Note the typical parabolic shape of the reconstructed ice sheets and the different extent and height of the ice sheet at each shield.

Table 3. Results of Ice Sheet Profile Reconstructions for the Tharsis Montes

Model	Arsia	Pavonis	Ascraeus
Fastook et al. [2004] model[a]	2.0–2.1	-	-
H_M, MOLA profile,[b] km	2.4	2.2	1.6
H_{FP}, flat plane, km	3.5	2.4	1.6
Difference, $H_{FP} - H_M$, km	1.1 (31%)	0.2 (8%)	-

[a]The *Fastook et al.* [2004] model was only used for reconstructions at Arsia Mons.

[b]All values represent average ice thickness in kilometers for the reconstructed profiles. Reconstructions with a steady state, perfectly plastic profile model [*Denton and Hughes*, 1981] were completed for each of the Tharsis Montes using a MOLA topography base and a flat plane base to evaluate the influence of the local topography on equilibrated ice thickness. The results indicate that shallow slopes (<1.0°) can greatly affect ice thicknesses under these conditions.

[88] Rough estimates for the volume of water ice necessary to form these glaciers can be obtained using the profile thickness estimates (Table 3) and the total surface area covered by the fan-shaped deposits (Table 1). These calculations suggest that the amount of water ice necessary to form the Tharsis Montes glaciers is approximately 13–19% of the total volume of both polar caps ($3.2–4.7 \times 10^6$ km^3 [*Smith et al.*, 1999]). Future map-plane, ice sheet reconstructions of the Tharsis Montes glaciers will provide more accurate estimates of the total volume of water ice necessary for their formation.

5. Potential Formative Mechanism for Tharsis Montes Glaciers

5.1. Evolution of Mars Orbital Parameters

[89] During the past 20 years, an improved understanding of Mars orbital dynamics and the development of comprehensive general circulation models of the Martian atmosphere have allowed for significant advances in Mars climatology. At present, Mars' obliquity is 25.19° and its eccentricity is 0.093 with perihelion occurring near the northern winter solstice at $L_s = 250°$ [*Haberle et al.*, 2003]. However, the orbit of Mars experiences predictable, periodic cycles for obliquity, eccentricity, and precession (L_s of perihelion). Mars lacks a large moon and is strongly perturbed by relatively nearby Jupiter; consequently its obliquity and eccentricity vary much more than they do for the Earth [*Haberle et al.*, 2003]. Precession has a period of ~51,000 years, obliquity has a period of ~120,000 years, and eccentricity, a period of ~95,000–99,000 years, with a strong modulation period of 2.4 million years [*Laskar et al.*, 2002]. Of these three orbital parameters, variations in obliquity exert the strongest influence on the climate system of Mars [*Haberle et al.*, 2003].

[90] During the past 10 Myr, Mars has experienced periodic obliquity cycles ranging from approximately 13°–42° with a period of around 1.2×10^5 years (Figure 29) [*Ward*, 1992]. Original attempts to extend obliquity models beyond this time period resulted in chaotic variation between 0° and 60° [*Laskar and Robutel*, 1993; *Touma and Wisdom*, 1993]. However, new unique solutions for obliquity and precession of the Mars axis for the past 10–20 Myr were computed using initial conditions deduced from the Pathfinder mission (Figure 29) [*Laskar et al.*, 2002, 2004]. Extended calculations for the past 250 Myr allow for a derivation of statistical data for the chaotic system, yielding precise estimates of the density probability functions for evolution of eccentricity and obliquity of Mars [*Laskar et al.*, 2004]. The results of this 250 Myr analysis show that the mean obliquity for Mars during this time period is 34.6°, with a range of 0.04°–66.15° and a standard deviation of 9.97° [*Laskar et al.*, 2004]. These estimates are critical for the formation and evolution of the Tharsis Montes glaciers, considering that age estimates for the fan-shaped deposits range from a few Myr to a few hundred Myr.

5.2. Predicted Effects of Orbital Parameters on Climate

[91] Under the current orbital configuration for Mars, climate conditions are such that water ice is unstable on the surface in the equatorial regions year-round [*Farmer and Doms*, 1979; *Mellon and Jakosky*, 1993]. However, it has been suggested that water ice may theoretically be stable at the surface under current conditions within the Tharsis rise due to the low thermal inertia of the soil, increased elevation and the lower mean annual temperature of the region [*Carr*, 1996]. In addition, changes in obliquity alter the latitudinal variation of solar insolation. The poles receive an increasing amount of insolation as the obliquity increases, while equatorial insolation decreases [*Jakosky and Carr*, 1985; *Haberle et al.*, 2003]. Above 54° obliquity, the poles receive more annual average insolation than the equator [*Haberle et al.*, 2003]. Such changes in the pattern of insolation can have a profound effect on ground temperatures, the distribution of volatiles around the planet, and the frequency and location of dust storms [*Haberle et al.*, 2003]. Under these conditions, significant evaporative loss of any volatiles at the poles would occur [*Jakosky and Carr*, 1985], increasing the atmospheric volatile content and lowering mean annual temperatures in the equatorial regions [*Mellon and Jakosky*, 1993], eventually resulting in local saturation and precipitation at cold traps. Thus, at high obliquities (>35°), significant amounts of water can be transported equatorward and deposited as ice at low latitudes

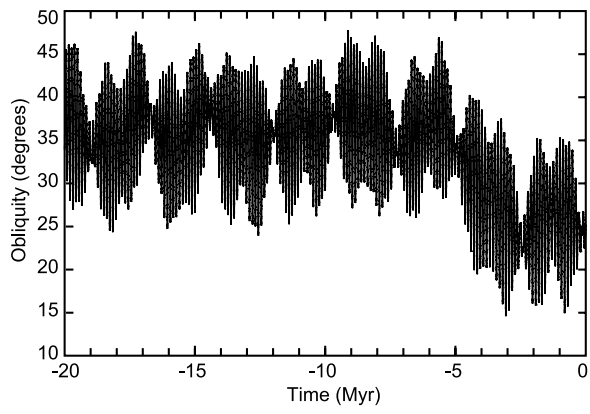

Figure 29. Plot of Mars obliquity variations over the past 20 Myr [from *Laskar et al.*, 2004]. Note the significant increase in mean obliquity from ~25° to ~36° at about 5 Ma. The Tharsis Montes glaciers likely formed during periods of increased mean obliquity as was the case a few tens of Myr.

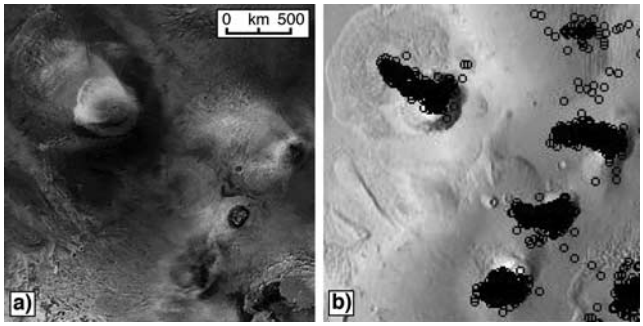

Figure 30. (a) Mars Global Surveyor daily global image mosaic taken April 1999 during a northern summer day. Bluish-white water ice clouds are present to the northwest of each of the Tharsis Montes (Image credit NASA/JPL/MSSS PIA02066). (b) Cumulative plot of cloud center location in daily global images (marked by circles) over one and a quarter Martian years (15 March 1999 to 31 July 2001) by *Benson et al.* [2003]. Under current climate conditions, water ice clouds consistently form over the summit and western flanks of the Tharsis Montes and Olympus Mons. See color version of this figure in the HTML.

[*Jakosky and Carr*, 1985]. For obliquities of ~45°, predicted sublimation rates at the north polar cap become so large (~10 cm/yr) that the whole cap may be evaporated in about 10,000 years unless a dark residual deposit acts as a sublimation barrier [*Jakosky et al.*, 1995; *Laskar et al.*, 2002].

5.3. General Climate Model Simulations at High Obliquity

[92] As initially predicted by *Jakosky and Carr* [1985], recent numerical models confirm that under periods of higher obliquity, the latitudes of stable, perennial ice are greatly affected [*Mischna et al.*, 2003]. By modifying Mars general circulation models to account for the effects of obliquity variations, estimates for latitudinal locations and amounts of precipitation can be obtained [*Richardson and Wilson*, 2002; *Mischna et al.*, 2003; *Haberle et al.*, 2004]. For an obliquity angle of 45°, *Richardson and Wilson* [2002] found that ice remains stable year-round at the equator and that within only three simulated Martian years a band of permanent ice began to develop at latitudes of 10°–20° N due to overlapping of much more extensive water ice caps. These results were confirmed by the general circulation model used by *Mischna et al.* [2003] who found that the stable location of surface ice moves equatorward with increasing obliquity, such that by 45° obliquity, water ice is stable year-round in the tropics only (between ~10°S–30°N) and permanent water ice accumulations (>20 cm) begin to develop within 30 Martian years. The water ice within this tropical surface ice belt is not spatially uniform, but rather greater accumulation occurs preferentially in regions of high topography [*Mischna et al.*, 2003], such as the Tharsis region. Simulations for extreme obliquity values (60°) show ubiquitous tropical coverage of surface ice at all longitudes during all seasons [*Mischna et al.*, 2003]. Recent high obliquity simulations using the Laboratoire de Meteorologie Dynamique and NASA/Ames GCMs show that water ice is transferred from the North pole of Mars to the flanks of the Tharsis volcanoes [*Haberle et al.*, 2004]. The permanent water ice accumulations predicted by these models are significant (rates of up to 16 cm a^{-1}) [*Haberle et al.*, 2004], and over sufficient timescales, glacial flow would be expected to occur.

[93] With atmospheric water vapor traveling toward the equator, it becomes apparent that a localized ice cap could have been enhanced by orographic effects on wind circulation [*Carr*, 1996]. Under these conditions, mountain wave clouds should form over each of the Tharsis Montes, possibly resulting in precipitation of volatiles if moisture content within the upward-moving air mass was sufficient. In a recent study by *Benson et al.* [2003], daily global maps utilizing wide-angle images captured by the Mars Orbiter Camera were analyzed for approximately one and a quarter Martian years to study water ice clouds in the Tharsis region. Observations of these clouds show that they tend to reside over each of the large Tharsis volcanoes during the northern summer, from about $L_s = 0°–220°$ with a peak at $L_s = 100°$. A cumulative plot of cloud centers shows that they cover the summit and more interestingly, the northwestern flanks of each of the three Tharsis Montes volcanoes and Olympus Mons (Figure 30) [*Benson et al.*, 2003]. With increased atmospheric volatile content during obliquity extremes, we would expect to see enhanced cloud formation and possibly precipitation in these same locations. The process by which nighttime mountain wave clouds form in the Martian atmosphere is outlined by *Colaprete and Toon* [2002]. Although their model was developed for CO_2 clouds, the mechanism for H_2O cloud formation is similar. The formative process for these clouds involves orographic uplift, whereby an air mass is forced upward due to a topographically significant obstacle on the surface. As the air mass continues to move upward, adiabatic cooling results in supersaturation and cloud particles begin to nucleate. If the volatile content of the air mass is relatively high, significant condensation will occur, resulting in the formation of large ice crystals [*Colaprete and Toon*, 2002]. When these particles reach a critical mass, they will begin to fall as precipitation. In a typical terrestrial environment, the orographic effect forces precipitation to fall on the windward side of the obstacle, effectively leaving the lee side in a "rain shadow." However, simulations of mountain wave clouds forming in the atmosphere of Mars at night reveal that a CO_2 "snow tail" actually forms on the leeward side of the obstacle [*Colaprete and Toon*, 2002]. This tail consists of ice particles formed at high altitudes that are blown downwind during their descent to the surface [*Colaprete and Toon*, 2002]. Applying this model to large obstacles such as the Tharsis Montes provides a mechanism by which significant amounts of precipitation of water ice could fall preferentially on the northwestern flanks of the shields. Taking this inference one step further suggests that prevailing winds at the time of precipitation were out of the east-southeast, resulting in deposition of volatiles on the west-northwestern flanks of the shields. These wind directions are consistent with GCM simulations at high obliquity, which predict east to west prevailing winds at low latitudes and winds out of the southeast in Tharsis [*Haberle et al.*, 2004]. On the other hand, if the volatiles necessary to form the cold-based glaciers of the Tharsis Montes were deposited

through a process similar to terrestrial orographic effects (i.e., deposition on the windward side due to rain shadow effect), the inferred wind direction would be reversed.

[94] Another possible mechanism for localized accumulation on the western flanks of the Tharsis Montes involves shielding of nighttime snowfall by daytime water ice clouds. Some GCM simulations at higher obliquities predict snowfall over most of the Tharsis region during the Martian night (M. I. Richardson, 2004, personal communication). However, warmer daytime temperatures in the Tharsis region prevent permanent water ice accumulations from forming in the simulations. An interesting scenario arises if daytime mountain wave clouds are also present over the summit and west-northwestern flanks of each of the Tharsis Montes volcanoes. These clouds could sufficiently reduce insolation to allow localized permanent snow accumulations to form over several diurnal cycles (M. I. Richardson, 2004, personal communication). However, this mechanism does not account for the large size differences of the three deposits or the lack of a large fan-shaped deposit at Olympus Mons. We believe that the "snow tail" model is the most plausible explanation for the location of the Tharsis Montes glaciers only on the west-northwestern side of each shield. Future GCM simulations at mesoscale resolutions with more advanced cloud microphysics may further constrain the mode of formation for the Tharsis Montes glaciers.

5.4. Deposit Formation and Present-Day Ice Content

[95] Assuming that these glaciers formed during a time when the Tharsis Montes were volcanically active, their composition would be influenced by erupted tephra [*Lucchitta*, 1981] in addition to atmospheric dust. Geologic timescales suggest that the Tharsis Montes were active well into the Mid to Late Amazonian period of Mars history [*Tanaka*, 1986]. We have also documented evidence that we believe represents a direct interaction between glacial and volcanic processes (i.e., arcuate scarps, possible subglacial volcanism) at Pavonis Mons, suggesting that the fan-shaped deposit formed during the late stages of volcanism at Pavonis. Eruptions occurring while a glacier was present on the flanks of the Tharsis Montes could deposit a significant amount of supraglacial tephra over the entire length of the glacier or specifically within the accumulation zone. It has also been suggested that higher atmospheric dust abundances would be expected during periods of higher obliquity [*Toon et al.*, 1980]. These dust particles could potentially act as condensation nuclei for water vapor in the atmosphere, resulting in rapid removal of dust and ice from the atmosphere to the surface [*Jakosky and Carr*, 1985]. Depending on the climatic conditions at the time, this debris could then be deposited through one of the mechanisms outlined earlier to form features within the fan-shaped deposits.

[96] The addition of a debris cover greatly inhibits the loss of water ice to the atmosphere at the surface, and we see evidence for a significant amount of unconsolidated debris within the fan-shaped deposits and surrounding areas. Sublimation rates and critical debris thickness necessary to preserve underlying ice on Mars are not well constrained; however, debris covers of <1 m are sufficient to severely inhibit sublimation in terrestrial analogs for Mars such as the Dry Valleys of Antarctica [*Marchant et al.*, 2002]. The residual deposit of the smooth facies at Pavonis Mons is hundreds of meters thick (Figure 16), suggesting that a significant ice component remains today. In addition, the ridged facies may represent ice-cored moraines, and the knobby facies may represent stagnant ice beneath an insulating debris cover. Thus the Pavonis Mons fan-shaped deposit could be a site where ancient glacial ice could potentially be preserved beneath a few meters of debris.

6. Age Estimates and Implications for Recent Climate Change on Mars

[97] Relative chronological systems have been established for the terrestrial planets through analysis of stratigraphic relationships and crater-counting statistics from remotely sensed data. With accurate absolute age estimates from isotopic analysis of samples, this relative timescale can be calibrated to an absolute timescale. Unfortunately, no in situ absolute sample ages are currently available for Mars. In addition to absolute ages provided by Martian meteorites, absolute ages from the Moon can be scaled to Mars using crater-production functions. This method relies on the assumption that the rate of production of craters on Mars of any given size is well-known for a certain time, and as a result the absolute crater retention age of different stratigraphic units on Mars can be estimated with an uncertainty factor of 2–3 [*Hartmann and Neukum*, 2001].

6.1. Previous Age-Dating Efforts

[98] *Tanaka* [1986] constrained the ages of the Tharsis Montes and Olympus Mons using stratigraphic relationships and Viking crater-counting data. All three of the Tharsis Montes were assigned a Late Amazonian age based on small lava flow units on the flanks as well as caldera and circumferential flank faults. *Tanaka* [1986] also considered the fan-shaped deposits of the Tharsis Montes and Olympus Mons, noting that the "landslide materials along the basal scarp of Olympus Mons are superposed on Late Amazonian lava flows" and the "concentric ridged debris blankets on the western flanks of the Tharsis Montes are about the same age as the volcanoes' youngest flows" [*Scott and Tanaka*, 1981; *Tanaka*, 1986].

[99] Crater-counting efforts by *Zimbelman and Edgett* [1992] confirm that Arsia Mons is the oldest of the three Tharsis Montes and Ascraeus is the youngest [*Blasius*, 1976; *Plescia and Saunders*, 1979; *Neukum and Hiller*, 1981]. However, no craters with visible ejecta deposits were observed on Pavonis Mons and the criteria of *Blasius* [1976] proved difficult to apply to the more moderate-resolution Viking images of Pavonis and Arsia Mons [*Zimbelman and Edgett*, 1992]. As a result of these difficulties, all stratigraphic assessments of *Zimbelman and Edgett* [1992] were derived solely from superposition relationships at unit contacts. The limited crater-frequency information prevented quantitative comparison of units with no spatial connections, such as correlations between similar units on different volcanoes [*Zimbelman and Edgett*, 1992].

[100] Regional mapping efforts of Arsia Mons by *Scott and Zimbelman* [1995] verify that the three facies of the fan-shaped deposits were emplaced throughout most of the Amazonian period. The knobby facies at Arsia Mons was tentatively assigned a Middle Amazonian age based on an

Table 4. THEMIS VIS Crater-Counting Statistics for N(0.063)–N(0.5) Within the Coverage of VIS Data[a]

Crater Diameter, m	Number of Craters, N_{cum}	Area, km^2	N_{cum}/km^2	Error
63	76	7000	1.09×10^{-2}	1.25×10^{-3}
125	19	7000	2.71×10^{-3}	6.23×10^{-4}
250	7	7000	1.00×10^{-3}	3.78×10^{-4}
500	0	7000	-	-

[a]Coverage is 7000 km^2, ~15% of the Pavonis fan-shaped deposit.

apparent embayment on the north side of the volcano by member 5 of the Tharsis Montes formation [*Scott and Zimbelman*, 1995]. However, this age is inconsistent with other stratigraphic relationships within the fan-shaped deposit and most likely stems from discrepancies associated with unit boundaries. The ridged facies at Arsia Mons clearly overlies member 5 and is therefore considered Late Amazonian age. Finally, the smooth facies is mapped as the youngest deposit at Arsia Mons.

[101] Regional mapping efforts of Pavonis Mons by *Scott et al.* [1998] indicate that most of the Pavonis shield is covered by Early Amazonian flows. The youngest lava flows of Late Amazonian age are relatively limited in extent, originating from a complex of faults and fissures on the northeastern and southwestern flanks of the volcano and the central caldera [*Scott et al.*, 1998]. *Scott et al.* [1998] state that "these flows were concurrent with, or closely followed, the emplacement of the fan-shaped deposit on the northwestern side of Pavonis Mons."

[102] Crater counts using high-resolution MOC images that included craters as small as ~16 m in diameter verify that the production function observed for young, well-preserved surfaces on Mars is the same as that found on the Moon [*Hartmann et al.*, 1999]. Crater-counting studies using MOC frames can yield more accurate dates for younger surfaces that lack large craters. On the basis of MOC crater counts, the Arsia Mons caldera was assigned an age of ~40–200 Ma with the outer flanks several times older (uncertainty factor of 2–3) [*Hartmann et al.*, 1999]. Later dating efforts based on larger craters gave ages of 200–400 Ma for the Arsia Mons caldera floor and 500–2000 Ma for the entire volcano flanks [*Hartmann and Neukum*, 2001]. Using counts of smaller diameter craters (45–700 m), a characteristic age of 100–200 Ma was assigned to Olympus Mons while age dating of craters larger than 700 m suggest an older age of 300–500 Ma [*Hartmann and Neukum*, 2001]. However, some MOC frames show individual flows with ages on the order of 10 Ma [*Hartmann and Neukum*, 2001], with additional dating of the youngest flows giving ages between 5 and 50 Ma [*Grier et al.*, 2001]. Analysis of recent data from the High Resolution Stereo Camera (HRSC) on board Mars Express provides similar age estimates for flows at Olympus Mons, with activity at ~115 Ma, ~25 Ma, and as recently as 2.4 Ma [*Neukum et al.*, 2004]. In the same study, crater counts for the fan-shaped deposit west of the Olympus Mons basal scarp yielded ages of 130–280 Ma with some subunits as young as 20–60 Ma [*Neukum et al.*, 2004].

6.2. New Crater-Counting Efforts

[103] While there are many limitations associated with crater-counting methodology, the absence of medium-resolution (10–200 meters/pixel) image data significantly limits the accuracy of absolute-age estimates derived with size-frequency plots. In addition, high-resolution MOC images can fit much younger isochrons than the average crater densities at larger diameters derived over larger areas from lower-resolution Viking images [*Hartmann and Neukum*, 2001]. The areal coverage of MOC images is also limited, potentially leading to misrepresentation of the true age for a particular geologic unit.

[104] The recent availability of THEMIS IR (100 meters/pixel) and THEMIS VIS (19 meters/pixel) data can serve to reduce uncertainties stemming from the resolution dichotomy in previously available data. New crater counts were performed for the Pavonis fan-shaped deposit using mosaics of THEMIS daytime IR and THEMIS VIS data. The THEMIS daytime IR mosaic coverage was approximately 73% of the total area of the Pavonis fan-shaped deposit while the VIS mosaic coverage was approximately 15% (Figure 5). Measurements were then made on individual craters observed within the daytime IR and VIS mosaics. Due to the limits of image resolution, craters <300 m in diameter within the IR mosaic were not counted and craters <50 m in the VIS mosaic were not counted. All craters observed within the Pavonis deposit had a diameter less than 1.0 km. Table 4 and Table 5 summarize these cumulative crater counts for the Pavonis fan-shaped deposit. These data points were then plotted on the *Hartmann and Neukum* [2001] isochrons to obtain age estimates for the Pavonis deposit (Figure 31).

6.3. Results

[105] Our crater-counting efforts for the Pavonis fan-shaped deposit confirm its Late Amazonian age. However, due to poor statistical distribution and limited coverage, it is difficult to derive an absolute age for the Pavonis deposit. When the data for craters N(0.063)–N(0.75) from THEMIS daytime IR and VIS images are plotted on the *Hartmann and Neukum* [2001] isochrons, they fall slightly above the 10 Ma isochrons (Figure 31). This suggests that the Pavonis fan-shaped deposit was formed between 10 Ma and 100 Ma. The N(0.063) and N(0.125) data points fall below this line, suggesting that some resurfacing and infilling of these smaller craters has occurred since their formation. However, without additional data points for craters smaller than 63 m or greater than 750 m in diameter, it is difficult to determine a specific absolute age range with confidence. In addition, several factors that would have influenced the crater-counting data must be considered. First, the units of the fan-shaped deposit are easily modified and appear to have undergone significant modification since their deposition. As a result, the entire deposit is expected to have a young crater-retention age. In addition, the characteristic size of

Table 5. THEMIS Daytime IR Crater-Counting Statistics for N(0.5)–N(1.0) Within the Coverage of Daytime IR Data[a]

Crater Diameter, m	Number of Craters, N_{cum}	Area, km^2	N_{cum}/km^2	Error
500	7	54,900	1.28×10^{-4}	4.82×10^{-5}
750	1	54,900	$1.82 \times 10-^{5}$	1.82×10^{-5}
1000	0	54,900	-	-

[a]Coverage is 54,900 km^2, ~73% of the Pavonis fan-shaped deposit.

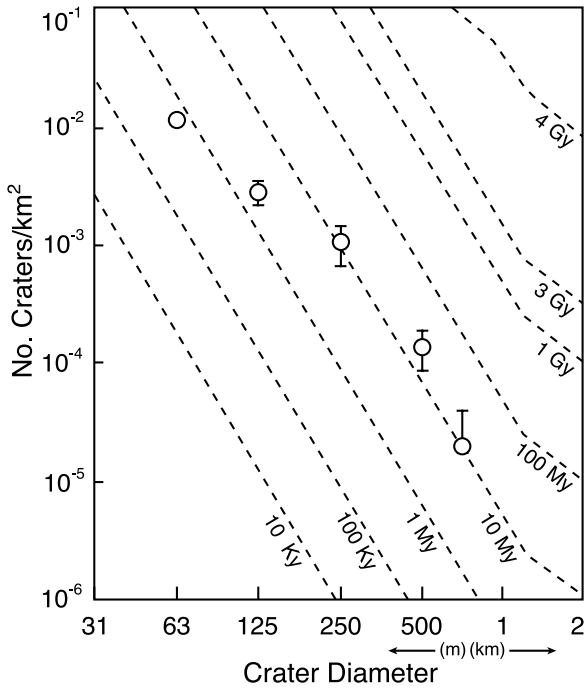

Figure 31. Crater-counting data N(0.063)–N(0.75) from THEMIS daytime IR and VIS mosaics for the Pavonis fan-shaped deposit plotted on the *Ivanov* [2001] isochrons derived from lunar crater count data by Neukum for R_{bolide} = 2.0 [*Hartmann and Neukum*, 2001]. No craters were observed with a diameter greater than 1 km. Uncertainty factor of ages is approximately 2 [*Hartmann and Neukum*, 2001]. See Figure 5 for the total coverage of THEMIS daytime IR and VIS images used for counts. The data fall slightly above the 10 Ma isochron and seem to indicate some resurfacing has taken place at smaller crater diameters. These counts in conjunction with analysis of mean obliquity values for Mars over the past 20 Myr suggest that the Pavonis fan-shaped deposit is >10 Ma and was probably formed a few tens of Myr to a few hundred Myr ago.

individual knobs and the general morphology of the knobby facies within the Pavonis deposit complicate crater identification within the knobby facies at the available resolutions. There are also many questionable circular features within the smooth facies at Pavonis that were not counted as craters based on the criteria of *Blasius* [1976]. Finally, at the THEMIS IR resolution (100 meters/pixel), there are several 300–600 m craters that appear to be fresh impacts into the ridged facies. However, THEMIS VIS images across the same craters reveal that they are actually impacts into the Tharsis lava plains underlying the thin veneer of the ridged facies. Thus some craters identified within the THEMIS daytime IR mosaic as impacts into the fan-shaped deposit may actually be underlying craters of the Tharsis lava plains, resulting in an overestimate for the age of the ridged facies. For all of these reasons, the superposition relationships of the fan-shaped deposits provide the most definitive age estimates of Late Amazonian age. Observations of lava and ice interaction during the evolution of the Pavonis fan-shaped deposit suggest that glaciation must have occurred concurrently with or prior to the estimated ages for the last phases of volcanism at Pavonis. Future counts of the flows adjacent to the scarps and margins of the fan-shaped deposit will help further constrain the maximum age for the deposits.

[106] Additional constraints for the age of these deposits can be derived through analysis of obliquity values during the past 20 Myr (Figure 29). Assuming that the Tharsis Montes glaciers formed during periods of higher mean obliquity than the current value, we can infer that they did not form in the past 5 Myr. Beyond 5 Ma, the mean obliquity for Mars increases to around 35°, providing conditions under which these glaciers could potentially have formed. Unfortunately, extending the solutions for the obliquity of Mars beyond 20 Ma results in chaotic behavior [*Laskar et al.*, 2004], and it is difficult to correlate one particular set of conditions with the formation of the Tharsis Montes glaciers. Despite this limitation, combining the obliquity constraints with the crater-counting data provides a minimum age of >10 Ma for the Pavonis fan-shaped deposit, while the maximum age estimates remain poorly constrained at a few hundred Myr. These Late Amazonian age estimates for the Pavonis fan-shaped deposit are consistent with estimates for the larger lobes of the Olympus Mons fan-shaped deposit (130–280 Ma [*Neukum et al.*, 2004]), suggesting that the two deposits share a similar timescale for formation.

7. Discussion

[107] Using Viking Orbiter data, *Edgett* [1989] completed an excellent, comprehensive review of previous work involving the Tharsis Montes fan-shaped deposits. This objective review provides a thorough summary of the prominent explanations for the fan-shaped deposits that proved to be critical during our analysis of new data. As part of this review, arguments for and against both the landslide and glacial hypotheses were outlined; however, no final conclusion regarding their origin was reached. A review of the landslide hypothesis was presented in the introductory section of this paper. Here, we consider each of the objections to the glacial hypothesis put forth by *Edgett* [1989], specifically "unless polar wandering hypotheses [*Schultz and Lutz*, 1988] are to be believed, there is little reason to suspect that glaciers/icecaps could have formed these features," because of the following:

[108] 1. "They do not resemble landforms found near the polar caps."

[109] The cold-based glaciers that formed the Tharsis Montes fan-shaped deposits would not be expected to produce the same landforms as the current polar caps. The Tharsis Montes glaciers formed at high elevations on the flanks of their respective volcanoes, flowed downslope and laterally expanded upon reaching the break in slope onto surrounding plains. This type of ice behavior is often classified as a piedmont glacier in terrestrial environments [*Benn and Evans*, 1998]. The Martian polar caps have formed on relatively flat regions, resulting in a continental ice sheet which expands outward in all directions. The scale, behavior, and resulting landforms of these two types of glaciers are disparate on the Earth, and we would expect the same to hold true on Mars. In addition, the Tharsis Montes fan-shaped deposits are primarily depositional features of

glaciers, while the polar caps are "present" ice sheets, which may still be growing. We would not expect to see depositional features such as drop moraines around the polar caps because there is no evidence suggesting that the caps are currently retreating.

[110] 2. "They do not resemble proposed paleo-polar landforms [*Schultz and Lutz*, 1988]."

[111] The proposed paleo-polar landforms such as the Medusae Fossae Formation are locally much thicker than the Pavonis glacial features would have been. High-resolution images also reveal that the Medusae Fossae Formation appears highly degraded, indicating significant eolian modification has occurred, which would remove paleo-polar depositional features. As outlined before, we believe that obliquity variations, not true polar wander, are responsible for the deposition of water ice in the equatorial regions of Mars.

[112] 3. "All three volcanoes occur within 15 degrees latitude of the present equator."

[113] At obliquities greater than 35°, general circulation models have predicted deposition of water ice in the equatorial regions of Mars [*Jakosky and Carr*, 1985; *Richardson and Wilson*, 2002; *Mischna et al.*, 2003; *Haberle et al.*, 2004]. Under these conditions, low latitudes receive little insolation and serve as cold traps for water vapor in the atmosphere [*Jakosky and Carr*, 1985]. Furthermore, the increased elevation of the Tharsis Montes would serve to create isolated regions in the equatorial regions where deposition of water ice should occur before lower elevations at higher latitudes.

[114] 4. "The deposits occur at elevations from about 6–10 km, where the present atmospheric water vapor content is very low [*Farmer et al.*, 1977]."

[115] MOLA altimetry data reveal that the Pavonis deposit is observed with elevations between approximately 2.8–8.5 km, with >80% of the deposit below 4.5 km (Figure 7). At present, there may be little water vapor at these elevations; however, under previous atmospheric conditions, the location and percentage of the water vapor in the atmosphere would undoubtedly differ. Recent analysis of MGS daily global weather images document water ice clouds with top heights ranging from 12.0–14.0+ km at Pavonis Mons [*Benson et al.*, 2003]. These clouds typically cover the summit and the northwestern flanks of the three Tharsis Montes for most of the Martian year [*Benson et al.*, 2003]. Furthermore, atmospheric water does not necessarily need to be stable at the lower elevations of the fan-shaped deposits. If enough water ice were precipitated out at higher elevations on the flanks of the volcanoes, this ice would eventually begin to flow downslope to lower elevations and onto the surrounding terrain.

[116] 5. "Because these features seem to be among the youngest landforms in Tharsis, a glacial origin would require a very different Martian climate at a relatively recent time in history."

[117] These do appear to be some of the youngest features in Tharsis, forming during the Late Amazonian period in Mars history [*Scott et al.*, 1998]. It is important to point out that the fan-shaped deposits are only the depositional remains of glaciers; the actual formation of the glaciers could have occurred earlier in Martian history and large-scale retreat and deposition may have only occurred recently. However, obliquity variations of up to 45° are predicted to have occurred within the past 10^7 years at a frequency of approximately 10^5 years [*Ward*, 1992], with more extreme (up to 60°) obliquities occurring more than 10 Ma (Figure 29) [*Laskar and Robutel*, 1993; *Laskar et al.*, 2004]. During these obliquity cycles, GCM simulations predict that significant amounts of water ice are deposited in the equatorial regions, which could lead to the formation of these massive glaciers in relatively short periods of time.

[118] 6. "A glacial origin cannot adequately explain why the marginal ridges of the Arsia Mons lobe seem to pass undeflected through an impact crater and its ejecta [*Carr et al.*, 1977; *Lucchitta*, 1981]."

[119] These ridges are interpreted here as drop moraines, which are formed when supraglacial and englacial debris is deposited around the margins of a stagnant or retreating cold-based glacier. These moraines are minimally influenced by underlying topography such as impact craters or lava flows. Instead, they are passively draped over these features without deflection, as has been documented for terrestrial drop moraines found in the Antarctic Dry Valleys (Figure 12).

[120] 7. "There are some lobate features which seem to originate at fissures on the lower western flanks of Pavonis Mons, and these lobate features make up the hummocky portions of the Pavonis Mons [fan-shaped deposit]."

[121] Our interpretation proposes that the fan-shaped deposit at Pavonis Mons has a predominantly glacial origin while volcanism played a secondary role in its evolution. Our interpretation of the knobby (hummocky) facies involves vertical down-wasting of a large cold-based glacier, passively depositing a sublimation till on the underlying terrain. This is consistent with the observation that the knobby facies is draped over these lobate flow-like features, some of which have a relief of >500 m (Figures 13 and 18). As outlined earlier, these lobate features and nearby radial ridges may be the manifestation of early silicic flows predating glacial activity or subglacial eruptions that occurred beneath a glacier at Pavonis Mons. Subsequent down-wasting of the glacier would result in deposition of the knobby facies, which is draped over the flows and surrounding terrain.

8. Summary and Conclusions

[122] Each of the Tharsis Montes volcanoes has an Amazonian-aged fan-shaped deposit present on the west-northwestern flank. These deposits share three characteristic facies, including (1) a ridged facies, consisting of tens to >100 parallel, concentric ridges around the margins of the deposits, (2) a knobby facies composed of irregular hills and hummocks, and (3) a smooth facies of broad plains that superposes all other units within the deposits. We believe that the fan-shaped deposit at Pavonis Mons represents the depositional remains of a cold-based glacier that formed on the northwestern flanks and advanced onto the surrounding plains in recent Martian history. We interpret the ridged facies as drop moraines that formed around the margins of a retreating cold-based glacier, the knobby facies as a sublimation till formed during in situ vertical down-wasting of debris-rich ice, and the smooth facies as debris-covered remnant ice from the last major phase of glaciation at Pavonis Mons. Superposition relationships suggest that at least three

major phases of glaciation have occurred at Pavonis Mons. The topography of the smooth facies suggests that significant volumes of ice may still remain within the deposit. In addition, several unique features within the Pavonis deposit (i.e., large arcuate scarps, lobate flow-like features, and radial ridges) suggest that direct lava-ice interaction has taken place, possibly as subglacial volcanism. Little evidence for meltwater features was observed within the Pavonis fan-shaped deposit; however, a local group of candidate fluvial features is present along the northeastern boundary of the deposit.

[123] Ice sheet reconstruction efforts provide ice-thickness estimates for the Tharsis Montes glaciers (1.6–2.4 km) that are within the cold-based thermal regime, further supporting morphological observations and the cold-based glacial model. In addition, the location of the fan-shaped deposits is consistent with the local topography northwest of each shield, suggesting that the topography strongly influenced the overall distribution and orientation of the Tharsis Montes glaciers.

[124] The most plausible explanation for the presence of these tropical mountain glaciers involves formation through atmospheric deposition of water ice on the northwestern flanks of the Tharsis Montes during periods of high obliquity. Mars GCM simulations at high obliquity (>45°) predict that permanent water ice accumulations will form within a few Martian years in the Tharsis region. Additional modeling of the Martian atmosphere suggests that a "snow tail" should form over the Tharsis Montes on leeward slopes, providing a mechanism for water ice deposition solely on the west-northwestern flanks of each shield.

[125] Age estimates from crater size-frequency distribution plots and analysis of the mean obliquity for Mars over the past 20 Myr suggest that the Tharsis Montes glaciers probably formed within the past 10–200 Myr, indicating that significant climate change occurred in the Late Amazonian period of Mars history.

[126] **Acknowledgments.** We would like to thank J. Fastook, R. Parsons, S. Milkovich, C. Fassett, and J. Dickson for productive discussions and assistance. We gratefully acknowledge financial support from NASA MDAP grant NNG04GJ99G to J.W.H. and from the Brown University Royce Fellowship Program and NASA Rhode Island Space Grant Consortium to D.E.S. Thanks are extended to Richard Williams and Michael Carr for very helpful and constructive reviews.

References

Anguita, F., and F. Moreno (1992), Shear-induced folding in Arsia Mons aureole: Evidence for low-latitude Martian glaciations, *Earth Moon Planets*, *59*, 11–22.

Benn, D. I., and D. J. A. Evans (1998), *Glaciers and Glaciation*, 734 pp., Edward Arnold, London.

Benson, J. L., B. P. Bonev, P. B. James, K. J. Shan, B. A. Cantor, and M. A. Caplinger (2003), The seasonal behavior of water ice clouds in the Tharsis and Valles Marineris regions of Mars: Mars Orbiter Camera observations, *Icarus*, *165*, 34–52.

Blasius, K. R. (1976), The record of impact cratering on the great volcanic shields of the Tharsis region of Mars, *Icarus*, *29*(3), 343–361.

Bouchard, M. A. (1989), Subglacial landforms and deposits in central and northern Quebec, Canada, with an emphasis on Rogen moraines, *Sediment. Geol.*, *62*, 293–308.

Carr, M. H. (1996), *Water on Mars*, 229 pp., Oxford Univ. Press, New York.

Carr, M. H., R. Greeley, K. R. Blasius, J. E. Guest, and J. B. Murray (1977), Some Martian volcanic features as viewed from the Viking Orbiters, *J. Geophys. Res.*, *82*(28), 3985–4015.

Cas, R. A. F., and J. V. Wright (1987), *Volcanic Successions, Modern and Ancient: A Geological Approach to Processes, Products and Successions*, 528 pp., Allen and Unwin, St Leonards, NSW, Australia.

Clark, C. D., and R. T. Meehan (2001), Subglacial bedform geomorphology of the Irish ice sheet reveals major configuration changes during growth and decay, *J. Quat. Sci.*, *16*(5), 483–496.

Colaprete, A., and O. B. Toon (2002), Carbon dioxide snow storms during the polar night on Mars, *J. Geophys. Res.*, *107*(E7), 5051, doi:10.1029/2001JE001758.

Crumpler, L. S., and J. C. Aubele (1978), Structural evolution of Arsia Mons, Pavonis Mons and Ascreus Mons: Tharsis region of Mars, *Icarus*, *34*(3), 496–511.

Denton, G. H., and T. J. Hughes (1981), *The Last Great Ice Sheets*, 484 pp., John Wiley, Hoboken, N. J.

Edgett, K. S. (1989), The lobate features west of each of the Tharsis Montes, Mars: A re-evaluation of their origins, *Lunar Planet. Sci.*, *XX*(1), 256–257.

Edgett, K. S., and J. R. Zimbelman (1987), The geology of Pavonis Mons, Mars, *Lunar Planet. Sci.*, *XVIII*(1), 254–255.

Edgett, K. S., B. J. Butler, J. R. Zimbelman, and V. E. Hamilton (1996), Volatiles and volcanoes: Very late Amazonian ash deposits and explosive activity along the western flanks of the Tharsis Montes, Mars, *LPI Tech. Rep.*, *96*(1), pp. 13–14, Lunar and Planet. Inst., Houston, Tex.

Farmer, C. B., and P. E. Doms (1979), Global and seasonal water vapor on Mars and implications for permafrost, *J. Geophys. Res.*, *84*, 2881–2888.

Farmer, C. B., D. W. Davies, A. L. Holland, D. D. LaPorte, and P. E. Doms (1977), Mars: Water vapor observations from the Viking orbiters, *J. Geophys. Res.*, *82*(28), 4225–4248.

Fastook, J. L., J. W. Head, D. R. Marchant, and D. E. Shean (2004), Ice sheet modeling: Terrestrial background and application to Arsia Mons lobate deposit, Mars, *Lunar Planet. Sci.*, *XXXV*, abstract 1452.

Grier, J., W. Bottke, W. K. Hartmann, and D. C. Berman (2001), Mars: Chronological studies of the large volcanoes in Tharsis, *Lunar Planet. Sci.*, *XXXII*, abstract 1823.

Grizzaffi, P., and P. H. Schultz (1989), Isidis Basin: Site of ancient volatile-rich debris layer, *Icarus*, *77*, 358–381.

Haberle, R. M., J. R. Murphy, and J. Schaeffer (2003), Orbital change experiments with a Mars general circulation model, *Icarus*, *161*, 66–89.

Haberle, R. M., F. Montmessin, F. Forget, B. Levrard, J. W. Head, and J. Laskar (2004), GCM simulations of tropical ice accumulations: Implications for cold-based glaciers, *Lunar Planet. Sci.*, *XXXV*, abstract 1711.

Hartmann, W. K., and G. Neukum (2001), Cratering chronology and the evolution of Mars, *Space Sci. Rev.*, *96*, 165–194.

Hartmann, W. K., M. Malin, A. McEwen, M. Carr, L. Soderblom, P. Thomas, E. Danielson, P. James, and V. Joseph (1999), Evidence for recent volcanism on Mars from crater counts, *Nature*, *397*(6720), 586–589.

Head, J. W., and D. R. Marchant (2003), Cold-based mountain glaciers on Mars: Western Arsia Mons, *Geology*, *31*(7), 641–644.

Head, J. W., et al. (2005), Tropical to mid-latitude snow and ice accumulation flow and glaciation on Mars, *Nature*, *434*, 346–351.

Helgason, J. (1999), Formation of Olympus Mons and the aureole-escarpment problem on Mars, *Geology*, *27*(3), 231–234.

Hodges, C. A., and H. J. Moore (1994), Atlas of volcanic landforms on Mars, *U.S. Geol. Surv. Prof. Pap.*, *1534*, 26–38.

Ivanov, B. A. (2001), Mars/Moon cratering rate ratio estimates, *Space Sci. Rev.*, *96*, 87–104.

Jakosky, B. M., and M. H. Carr (1985), Possible precipitation of ice at low latitudes of Mars during periods of high obliquity, *Nature*, *315*(6020), 559–561.

Jakosky, B. M., B. G. Henderson, and M. T. Mellon (1995), Chaotic obliquity and the nature of the Martian climate, *J. Geophys. Res.*, *100*(E1), 1579–1584.

Laskar, J., and P. Robutel (1993), The chaotic obliquity of the planets, *Nature*, *361*(6413), 608–612.

Laskar, J., B. Levrard, and J. F. Mustard (2002), Orbital forcing of the Martian polar layered deposits, *Nature*, *419*(6905), 375–377.

Laskar, J., A. C. M. Correia, M. Gastineau, F. Joutel, B. Levrard, and P. Robutel (2004), Long term evolution and chaotic diffusion of the insolation quantities of Mars, *Icarus*, *170*, 343–364.

Lewis, W. V. (1940), Dirt cones on the northern margins of Vatnajokull, Iceland, *J. Geomorphol.*, *3*, 16–26.

Lucchitta, B. K. (1981), Mars and Earth: Comparison of cold-climate features, *Icarus*, *45*, 264–303.

Marchant, D. R., A. R. Lewis, W. M. Phillips, E. J. Moore, R. A. Souchez, G. H. Denton, D. E. Sugden, N. Potter Jr., and G. P. Landis (2002), Formation of patterned ground and sublimation till over Miocene glacier ice in Beacon Valley, southern Victoria Land, Antarctica, *Geol. Soc. Am. Bull.*, *114*(6), 718–730.

Mellon, M. T., and B. M. Jakosky (1993), Geographic variations in the thermal and diffusive stability of ground Ice on Mars, *J. Geophys. Res.*, *98*(E2), 3345–3364.

Milkovich, S. M., and J. W. Head (2003), Olympus Mons fan shaped deposit morphology: Evidence for debris glaciers, in *Sixth International Conference on Mars*, abstract 3149, Lunar and Planet. Inst., Houston, Tex.

Mischna, M. A., M. I. Richardson, R. J. Wilson, and D. J. McCleese (2003), On the orbital forcing of Martian water and CO_2 cycles: A general circulation model study with simplified volatile schemes, *J. Geophys. Res.*, *108*(E6), 5062, doi:10.1029/2003JE002051.

Morris, A., P. Mouginis-Mark, and S. Baloga (2003), Did glaciers exist recently on the Tharsis Montes?, *Eos Trans. AGU*, *84*(46), Fall Meet. Suppl., Abstract P32C-08.

Muhleman, D. O., B. J. Butler, A. W. Grossman, and M. A. Slade (1991), Radar images of Mars, *Science*, *253*(5027), 1508–1513.

Neukum, G., and K. Hiller (1981), Martian ages, *J. Geophys. Res.*, *86*, 3097–3121.

Neukum, G., and D. U. Wise (1976), Mars: A standard crater curve and possible new time scale, *Science*, *194*(4272), 1381–1387.

Neukum, G., et al. (2004), Recent and episodic volcanic and glacial activity on Mars revealed by the High Resolution Stereo Camera, *Nature*, *432*(7020), 971–979.

Nye, J. F. (1952), A method of calculating the thicknesses of the ice-sheets, *Nature*, *169*(4300), 529–530.

Parsons, R. L., and J. W. Head (2004), Ascraeus Mons, Mars: Characterisation and interpretation of the fan-shaped deposit on its western flank, *Lunar Planet. Sci.*, *XXXV*, abstract 1776.

Plescia, J. B., and S. R. Saunders (1979), The chronology of the Martian volcanoes, *Lunar Planet. Sci.*, *X*, 2841–2859.

Rains, R. B., and J. Shaw (1981), Some mechanisms of controlled moraine development, Antarctica, *J. Glaciol.*, *27*(95), 113–128.

Reeh, N. (1982), A plasticity theory approach to the steady-state shape of a three-dimensional ice sheet, *J. Glaciol.*, *28*(100), 431–455.

Richardson, M. I., and R. J. Wilson (2002), Investigation of the nature and stability of the Martian seasonal water cycle with a general circulation model, *J. Geophys. Res.*, *107*(E5), 5031, doi:10.1029/2001JE001536.

Schultz, P. H., and A. B. Lutz (1988), Polar wandering of Mars, *Icarus*, *73*, 91–141.

Scott, D. H., and K. L. Tanaka (1981), Mars: Paleostratigraphic restoration of buried surfaces in Tharsis Montes, *Icarus*, *45*, 304–319.

Scott, D. H., and K. L. Tanaka (1986), Geologic map of the western equatorial region of Mars, *U.S. Geol. Surv. Misc. Invest. Ser.*, *Map I-1802–A*.

Scott, D. H., and J. R. Zimbelman (1995), Geologic map of Arsia Mons Volcano, Mars, *U.S. Geol. Surv. Misc. Invest. Ser.*, *Map I-2480*.

Scott, D. H., J. M. Dohm, and J. R. Zimbelman (1998), Geologic map of Pavonis Mons Volcano, Mars, *U.S. Geol. Surv. Misc. Invest. Ser.*, *Map I-2561*.

Smith, D. E., et al. (1999), The global topography of Mars and implications for surface evolution, *Science*, *284*(5419), 1495–1503.

Smith, D. E., et al. (2001), Mars Orbiter Laser Altimeter: Experiment summary after the first year of global mapping of Mars, *J. Geophys. Res.*, *106*(E10), 23,689–23,722.

Soderblom, L. A. (1977), Historical variations in the density and distribution of impacting debris in the inner solar system; evidence from planetary imaging, in *Impact and Explosion Cratering: Planetary and Terrestrial Implications: Proceedings of the Symposium on Planetary Cratering Mechanics*, edited by D. J. Roddy, R. O. Pepin, and R. B. Merrill, pp. 629–633, Elsevier, New York.

Swithinbank, C. (1950), The origin of dirt cones on glaciers, *J. Glaciol.*, *1*(8), 461–465.

Tanaka, K. L. (1986), The stratigraphy of Mars, *J. Geophys. Res.*, *91*(B13), E139–E158.

Toon, O. B., J. B. Pollack, W. Ward, J. A. Burns, and K. Bilski (1980), The astronomical theory of climate change on Mars, *Icarus*, *44*, 552–607.

Touma, J., and J. Wisdom (1993), The chaotic obliquity of Mars, *Science*, *259*(5099), 1294–1297.

Ward, W. R. (1992), Long-term orbital and spin dynamics of Mars, in *Mars*, edited by H. H. Kieffer et al., pp. 298–320, Univ. of Ariz. Press, Tucson.

Williams, R. S. (1978), Geomorphic processes in Iceland and on Mars: A comparative appraisal from orbital images, *Geol. Soc. Am. Abstr. Programs*, *10*, 517.

Wilson, L., and J. W. Head (2002), Heat transfer and melting in subglacial basaltic volcanic eruptions: Implications for volcanic deposit morphology and meltwater volumes, in *Volcano-Ice Interaction on Earth and Mars*, edited by J. L. Smellie and M. G. Chapman, *Geol. Soc. Spec. Publ.*, *202*, 5–26.

Zimbelman, J. R., and K. S. Edgett (1992), The Tharsis Montes, Mars: Comparison of volcanic and modified landforms, *Lunar Planet Sci.*, *XXII*, 31–44.

Zuber, M. T., et al. (2000), Internal structure and early thermal evolution of Mars from Mars Global Surveyor topography and gravity, *Science*, *287*, 1788–1793.

J. W. Head and D. E. Shean, Department of Geological Sciences, Brown University, Box 1846, Providence, RI 02912, USA. (james_head_III@brown.edu)

D. R. Marchant, Department of Earth Sciences, Boston University, Boston, MA 02215, USA.